Doped moiré magnets: Renormalized flat bands and excitonic phases

Ilia Komissarov,[1,*] Onur Erten,[2,†] and Pouyan Ghaemi[3,4,‡]
[1]*Department of Physics, Columbia University, New York, New York 10027, USA*
[2]*Department of Physics, Arizona State University, Tempe, Arizona 85287, USA*
[3]*Physics Department, City College of the City University of New York, New York, New York 10031, USA*
[4]*Physics Program, Graduate Center of City University of New York, New York, New York 10031, USA*

(Received 3 September 2024; revised 14 November 2024; accepted 2 December 2024; published 13 December 2024)

We explore the phase diagram of a twisted bilayer of strongly interacting electrons on a honeycomb lattice close to half filling using the slave-boson mean-field theory. Our analysis indicates that a variety of new phases can be realized as a function of chemical doping and twist angle. In particular, we find a nonmagnetic excitonic insulating phase that breaks the translational symmetry of the underlying moiré pattern. This phase results from the interplay of strong Coulomb interactions and the twist angle. In addition, we show that the features of the renormalized dispersion, such as the magic angles, depend significantly on the interactions. Our results highlight the rich physics arising in doped moiré superlattices of Mott insulators.

DOI: 10.1103/PhysRevB.110.245126

I. INTRODUCTION

The discovery of superconductivity in twisted bilayer graphene [1] has sparked extensive research into moiré superlattices. The quantum interference of electronic wave functions in twisted or misaligned bilayers leads to the suppression of the kinetic energy of electrons relative to the electron-electron interaction energy. By leveraging the high tunability of such platforms, much effort is made to explore and control correlated electronic phases of matter [2–4], which have long been a complex and intriguing area of research [5]. Correlated phases of matter can also be realized in bulk d- and f-electron materials such as cuprates [6] or heavy fermions [7]. In these systems, the strong electron-electron interaction surpasses the kinetic energy due to the absence of screening. The correlated electronic states realized via the twisting share many similarities with these phases. However, some important differences are notable [8].

While moiré engineering of electronic phases in weakly correlated layers such as semiconductors and graphene has been extensively studied, the research on the moiré superlattices composed of Mott insulators and magnets is at its seminal stages. To date, a limited number of theoretical investigations on moiré superlattices of magnetic materials have been conducted [9–17]. Several of these predicted phases have been demonstrated experimentally [18–20]. One prominent example of such a platform is the twisted cuprates where the Dirac spectrum emerges with the formation of the Bogoliubov quasiparticle excitations of the d-wave superconducting phases [21–25].

In this article, we explore the venue of small twist angle bilayers of honeycomb materials with strong Coulomb repulsion [26] described by the t-J model [27,28]. Our study is motivated by the observation that many two-dimensional Mott insulators with novel magnetic quantum phases possess a honeycomb lattice structure [29]. Contrary to the twisted noninteracting materials, where the nontrivial correlated states are stabilized in a narrow range of dopings close to Fermi energy [30], in the system considered here, due to the strong interactions in each layer, electronic states in a wide range of energies participate in the formation of the ground state. In this aspect, our approach is essentially different from the commonly used approximation that utilizes the projection into the flat topological bands at charge neutrality. Here, we use the entire band structure of the interacting continuum model, and the obstruction to the Wannierization present in the low-lying Chern bands is avoided. This sacrifices some of the ultraviolet details of the band structure due to the truncation of the Brillouin zone but preserves the physical picture of the local moments.

Our results show that twisted doped Mott insulators can host new types of quantum phases, one example of which is an excitonic insulator of spinons. The emergence of this phase is crucially related to both strong correlations in each layer and the relative twist of the two layers, which produces the moiré minibands. Within our mean-field analysis, the gaps between the minibands are controlled by the interactions, which enables the stabilization of the nonmagnetic insulating phases when the Fermi level lies in one of such gaps. This excitonic insulator originates from the finite momentum hybridization of the interlayer spinons and breaks the translation symmetry of the underlying moiré lattice while the intralayer order parameters stay homogeneous.

The rest of the paper is organized as follows. In Sec. II, we describe the parton mean-field theory for the strongly interacting hexagonal bilayer. Section III details the phase

*Contact author: i.komissarov@columbia.edu
†Contact author: onur.erten@asu.edu
‡Contact author: pghaemi@ccny.cuny.edu

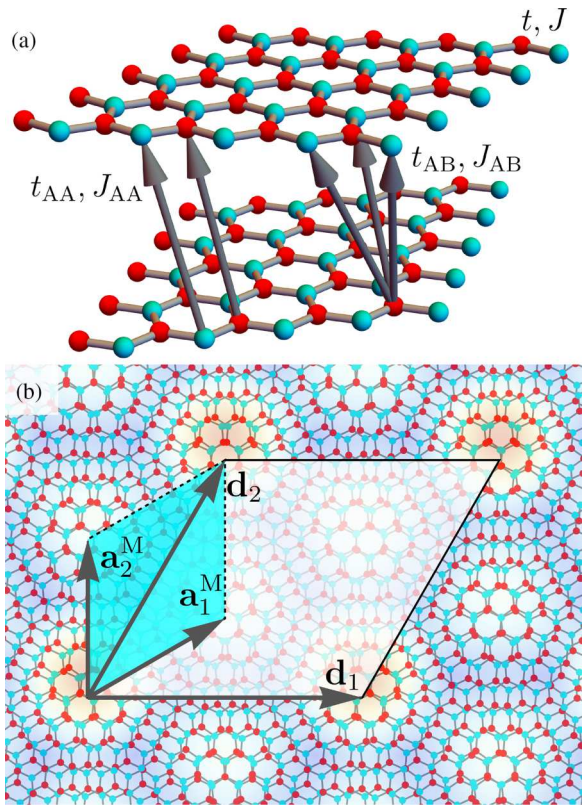

FIG. 1. (a) The depiction of a twisted bilayer doped Mott insulator with the intra- and interlayer hopping and superexchange parameters. The intralayer hopping and superexchange are denoted with t and J. The interlayer hoppings (superexchange) terms considered are indicated with arrows: J_{AA} and t_{AA} correspond to AA and BB terms, and J_{AB} and t_{AB} interpolate between different sublattices of different layers. (b) At high values of the interlayer superexchange J_{AA} and sufficient hole doping $\mu_0 < 0$, the ground state of the system is the excitonic insulator of spinons characterized by the nonzero values of the order parameter $\chi_{AA(BB)} = \langle \hat{f}^{(1)\dagger}_{A(B)} \hat{f}^{(2)}_{A(B)} \rangle$, which breaks the translation symmetry of the moiré lattice as indicated. The area of the unit cell in this phase (shaded with white) is three times larger than the area of the hexagonal moiré unit cell (shown with blue), and the lattice vectors in the real space are promoted from $\mathbf{a}_1^M$ and $\mathbf{a}_2^M$ to $\mathbf{d}_1$ and $\mathbf{d}_2$.

diagram of the slave-boson mean-field theory. Some aspects peculiar to the twisted bilayers, such as the magic angles and the twist-angle dependence of the phases, are also discussed. We conclude with a summary of our results and an outlook in Sec. IV.

II. MODEL AND METHODS

We consider a twisted honeycomb bilayer as depicted in Fig. 1(a). Assuming the limit of strong Coulomb interactions and small doping, we use the following t-J model, which captures both inter- and intralayer interactions:

$$\hat{H}_{t-J} = -\sum_{\langle ij \rangle} t_{ij} \hat{P} \hat{c}^\dagger_{i\sigma} \hat{c}_{j\sigma} \hat{P} + \sum_{\langle ij \rangle} J_{ij} \left(\hat{\mathbf{S}}_i \cdot \hat{\mathbf{S}}_j - \frac{1}{4} \hat{n}_i \hat{n}_j \right) - \mu_0 \sum_i \hat{c}^\dagger_{i\sigma} \hat{c}_{i\sigma}. \quad (1)$$

Here, we define $t_{ij} \equiv t$ and $J_{ij} \equiv J$ for the indices i, j belonging to the neighboring cites of the honeycomb lattice in the same layer. The interlayer hoppings and magnetic couplings have the forms $t_{ij} = t_{AA}(|i-j|)$ and $J_{ij} = J_{AA}(|i-j|)$ for i, j belonging to the same sublattice in both layers whereas $t_{ij} = t_{AB}(|i-j|)$, $J_{ij} = J_{AB}(|i-j|)$ when i, j belong to opposite sublattices in the two layers. We assume that $t_{AA} = t_{BB}, t_{AB}$, $J_{AA} = J_{BB}, J_{AB}$ are smooth functions of their argument, which justifies using the interacting analog of the Bistritzer-MacDonald model [31].

The spin operators are expressed in terms of Abrikosov fermions as $\hat{\mathbf{S}}_i = \frac{1}{2} \sum_{\sigma\sigma'} \hat{f}^\dagger_{i\sigma} \boldsymbol{\sigma}_{\sigma\sigma'} \hat{f}_{i\sigma'}$, where $\boldsymbol{\sigma}$ is a vector of Pauli matrices and $\hat{P}$ denotes the projector into the subspace of singly occupied sites. We implement the single-occupancy constraint via slave-boson formalism [32]

$$\hat{c}_{i\sigma} = \hat{b}^\dagger_i \hat{f}_{i\sigma}, \quad (2)$$

which leads to the holonomic condition

$$\sum_\sigma \hat{f}^\dagger_{i\sigma} \hat{f}_{i\sigma} + \hat{b}^\dagger_i \hat{b}_i = 1. \quad (3)$$

The relation above will be taken into account at the mean-field level by introducing into the Hamiltonian a corresponding term with a constant Lagrange multiplier λ. Within our mean-field analysis, we consider solutions with uniform holon occupation $\delta \equiv \langle \hat{b}^\dagger_i \hat{b}_i \rangle$. We further decouple the superexchange term in (1) in the direct and exchange channels as shown in Appendix A. In this work, we do not consider the superconducting state and retain the susceptibilities of the form $\chi_{ij} = \langle \hat{f}^\dagger_i \hat{f}_j \rangle$. The direct terms can be expressed in terms of δ through the constraint equation (3) (see Appendixes A and B). The resulting mean-field Hamiltonian can be written as

$$\hat{H} = \hat{H}_{\text{intra}} + \hat{H}_{\text{inter}} + (\lambda - \mu_0) \sum_{\mathbf{k}} \hat{f}^\dagger_{\mathbf{k}} \hat{f}_{\mathbf{k}} + C, \quad (4)$$

where

$$\hat{f}_{\mathbf{k}} = \left(\hat{f}^{(1)}_{\mathbf{k}A} \; \hat{f}^{(1)}_{\mathbf{k}B} \; \hat{f}^{(2)}_{\mathbf{k}A} \; \hat{f}^{(2)}_{\mathbf{k}B} \right), \quad (5)$$

and indices (1) and (2) denote the layer. The intralayer term is as follows:

$$(\hat{H}_{\text{intra}})_{\mathbf{Q}\mathbf{Q}'} = \delta_{\mathbf{Q}\mathbf{Q}'} \sum_{\mathbf{k}} \hat{f}^\dagger_{\mathbf{k}} H_{\text{intra}}(\mathbf{k}) \hat{f}_{\mathbf{k}}, \quad (6)$$

where $\mathbf{Q}$ and $\mathbf{Q}'$ lie within the moiré reciprocal lattice spanned by vectors $\boldsymbol{\Delta}_n$ (see Fig. 2). The contribution from the two valleys can be presented as follows:

$$H_{\text{intra}}(\mathbf{k}) = -\left(\delta t + \frac{\chi J}{4} \right) \begin{pmatrix} K^{(1)}_{\mathbf{k}} & 0 \\ 0 & K^{(2)}_{\mathbf{k}} \end{pmatrix}, \quad (7)$$

with the rotated hopping matrices

$$K^{(l)}_{\mathbf{k}} = v_F [R(\pm\theta/2)(\mathbf{k} + \mathbf{Q}) \cdot (\hat{\sigma}_x, \hat{\sigma}_y)], \quad v_F = \tfrac{3}{2} a t, \quad (8)$$

where we set the lattice constant a equal to unity. The interlayer Hamiltonian $\hat{H}_{\text{inter}}$ is a sum of the hopping $\hat{H}^t_{\text{inter}}$ and superexchange $\hat{H}^J_{\text{inter}}$ components as introduced here:

$$(\hat{H}_{\text{inter}})^{t(J)}_{\mathbf{Q}\mathbf{Q}'} = \sum_{\mathbf{k}\lambda nm} \hat{f}^\dagger_{\mathbf{k}} H^{t(J)}_{\text{inter},m\lambda} \hat{f}_{\mathbf{k}} \delta_{\mathbf{Q}-\mathbf{Q}', \lambda(\boldsymbol{\Delta}_m - \mathbf{q}^{t(J)}_n)}, \quad (9)$$

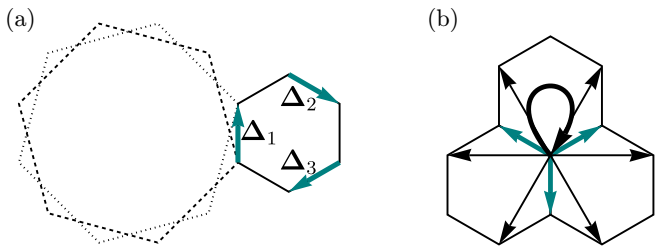

FIG. 2. (a) The small hexagon shows the moiré Brillouin zone; vectors $\mathbf{\Delta}_n$ connecting vertices on the moiré reciprocal lattice are indicated with blue arrows. (b) Three adjacent moiré Brillouin zones are shown together with blue arrows corresponding to vectors $\mathbf{\Delta}_n$ and indicating possible hybridization momenta of spinons in homogeneous superexchange case $\mathbf{q}_n^J = 0$. If this possibility is realized, both the terms $\hat{H}^t_{\text{inter}}$ and $\hat{H}^J_{\text{inter}}$ [see (9)] are of this type. The black arrows represent the hybridization possibilities entering the term $\hat{H}^J_{\text{inter}}$ in the case of spatially modulated superexchange $\mathbf{q}_n^J = \mathbf{\Delta}_n$. Note that in this case, every Dirac cone can hybridize with the Dirac cone from the other layer at the same point in the momentum space.

where $\lambda = \pm 1$ represent the hopping from layer 2 to layer 1, and the inverse process correspondingly, m and n run between 1 and 3, and $\mathbf{q}_n^t = 0$ [31]. Therefore, for $\hat{H}^t_{\text{inter}}$ the possible hybridization momenta between the states in different layers are always $\mathbf{\Delta}_n$, shown with blue arrows in Fig. 2.

Interlayer superexchange has a momentum dependence of the general form

$$\left\langle \hat{f}^{(1)\dagger}_{i\alpha} \hat{f}^{(2)}_{j\beta} \right\rangle = \chi_{\alpha\beta} \sum_{n=1}^{3} e^{i\mathbf{q}_n^J \cdot \mathbf{j}}. \tag{10}$$

We consider two possible mean-field solutions where $\mathbf{q}_n^J = 0$ and $\mathbf{q}_n^J = \mathbf{\Delta}_n$: in the latter choice, the interlayer hybridization momenta are modified by the momentum imparted by the spinon interlayer order parameters. The possible hybridization vectors in momentum space entering $\hat{H}^J_{\text{inter}}$ in this case are shown with black arrows in Fig. 2(b). The part of the Hamiltonian that corresponds to interlayer couplings assumes the form

$$H^t_{\text{inter},m\lambda} = \begin{pmatrix} 0 & T^t_m \\ 0 & 0 \end{pmatrix} \delta_{\lambda,1} + (\text{H.c.}) \delta_{\lambda,-1}, \tag{11}$$

$$H^J_{\text{inter},m\lambda} = \begin{pmatrix} 0 & T^J_m \\ 0 & 0 \end{pmatrix} \delta_{\lambda,1} + (\text{H.c.}) \delta_{\lambda,-1}, \tag{12}$$

$$T^t_m = -\begin{pmatrix} \delta t_{\text{AA}} & \omega^{m-1} \delta t_{\text{AB}} \\ \omega^{-(m-1)} \delta t_{\text{AB}} & \delta t_{\text{AA}} \end{pmatrix}, \tag{13}$$

$$T^J_m = -\begin{pmatrix} \frac{\chi_{\text{AA}} J_{\text{AA}}}{4} & \omega^{m-1} \frac{\chi_{\text{AB}} J_{\text{AB}}}{4} \\ \omega^{-(m-1)} \frac{\chi_{\text{AB}} J_{\text{AB}}}{4} & \frac{\chi_{\text{BB}} J_{\text{AA}}}{4} \end{pmatrix}, \tag{14}$$

where $\omega = e^{2\pi i/3}$. The constant term C found in (4) depends on the choice of $\mathbf{q}_m^J$ and can be found in Appendix B.

The mean-field Hamiltonian in (4) has similarities to the Bistritzer-MacDonald model describing the noninteracting bilayer of graphene [31] and possesses similar symmetries: C_6 rotations, moiré translations T_{M}, and the time reversal. When $\chi_{\text{AA}} \neq \chi_{\text{BB}}$, the C_2 symmetry is broken, and the K^{M} and $K^{\text{M}'}$ points located in the corners of the hexagonal moiré Brillouin zone become gapped. Another symmetry-breaking pattern corresponds to $\mathbf{q}_n^J \neq 0$. In the latter phase, if simultaneously $\delta \neq 0$, the moiré translation symmetry T_{M} is broken, and the unit cell in the real space triples as shown with white in Fig. 1(b).

The correlated twisted bilayer model has also some distinctive features compared to the noninteracting counterpart, which are captured by the self-consistency equations determining χ_{AA}, χ_{BB}, and χ_{AB} that we now address. The Fourier transform of the hopping term with momentum $\mathbf{K}$ equal to the distance to the K point acts as an interlayer hybridization parameter t_{AA} in the noninteracting Bistritzer-MacDonald model. Similarly, in our model, the corresponding superexchange $J_{\text{AA}} \equiv J^{\mathbf{K}}_{\text{AA}}$ is found as the Fourier transform of the function $J(|i-j|)$ at the momentum $\mathbf{K}$. However, besides $t_{\text{AA}} \equiv t^{\mathbf{K}}_{\text{AA}}$ and J_{AA}, the mean-field values of $\chi_{\text{AA(BB)}}$ depend on the Fourier transforms of $J(|i-j|)$ but at different momenta equal to either zero or to the reciprocal lattice vector

$$J^{\mathbf{0}}_{\text{AA}} = \int \frac{d^2\mathbf{r}}{\Omega} J(\mathbf{r}), \quad J^{\mathbf{G}}_{\text{AA}} = \int \frac{d^2\mathbf{r}}{\Omega} J(\mathbf{r}) e^{-i\mathbf{G}\cdot\mathbf{r}}, \tag{15}$$

as

$$\chi_{\text{AA}} = \frac{J^{\mathbf{K}}_{\text{AA}}}{J^{\mathbf{0}}_{\text{AA}}} \sum_{\mathbf{k},\, n<E_{\text{F}}} \langle n\mathbf{k}| \left(\hat{H}^J_{\text{inter}}\right)_{\text{AA}} |n\mathbf{k}\rangle \,, \tag{16}$$

in $\mathbf{q}_n^J = 0$ case, and

$$\chi_{\text{AA}} = \frac{J^{\mathbf{K}}_{\text{AA}}}{3\left(J^{\mathbf{0}}_{\text{AA}} + 2J^{\mathbf{G}}_{\text{AA}}\right)} \sum_{\mathbf{k},\, n<E_{\text{F}}} \langle n\mathbf{k}| \left(\hat{H}^J_{\text{inter}}\right)_{\text{AA}} |n\mathbf{k}\rangle \tag{17}$$

in the case of spatially nonuniform interlayer superexchange. With $|n\mathbf{k}\rangle$, we indicate the wave function of the full Hamiltonian $\hat{H}$ in miniband n at momentum $\mathbf{k}$, and $(\hat{H}^J_{\text{inter}})_{\text{AA}}$ denotes the interlayer hybridization Hamiltonian term (9) with all but AA matrix components set to zero (see Appendix B). Due to the prefactors in (16) and (17), the resulting phase diagram depends on the spread of the superexchange: the more it is localized in the real space, the larger the interlayer spinon condensates are, and the C_2-breaking phases are stabilized at the smaller values of J_{AA}.

We consider two types of *Ansätze* for the interlayer superexchange terms $\hat{H}^J_{\text{inter}}$: the uniform with $\mathbf{q}_n^J = 0$, and the $\mathbf{q}_n^J = \mathbf{\Delta}_n$. In the former case, the band structure of spinons is analogous to the one of the electrons in the Bistritzer-MacDonald model, as shown in Fig. 4(a). The latter choice triples the unit cell in real space leading to the appearance of an additional Dirac cone at the gamma point due to the folding of the moiré Brillouin zone, as shown in Fig. 4(b). If simultaneously $\chi_{\text{AA}} \neq \chi_{\text{BB}}$, C_2 symmetry is broken and all Dirac cones develop a gap, as indicated in Figs. 4(c)–4(e).

III. RESULTS AND DISCUSSION

By minimizing the Hamiltonian (4) with respect to the free parameters λ, δ, χ, χ_{AA}, χ_{BB}, χ_{AB}, and solving the resulting mean-field equations (see Appendix B) self-consistently, we obtain the phase diagram as presented in Fig. 3 in terms of the interlayer superexchange J_{AA} and the chemical potential μ_0. The breakdown of the phases with associated order parameters

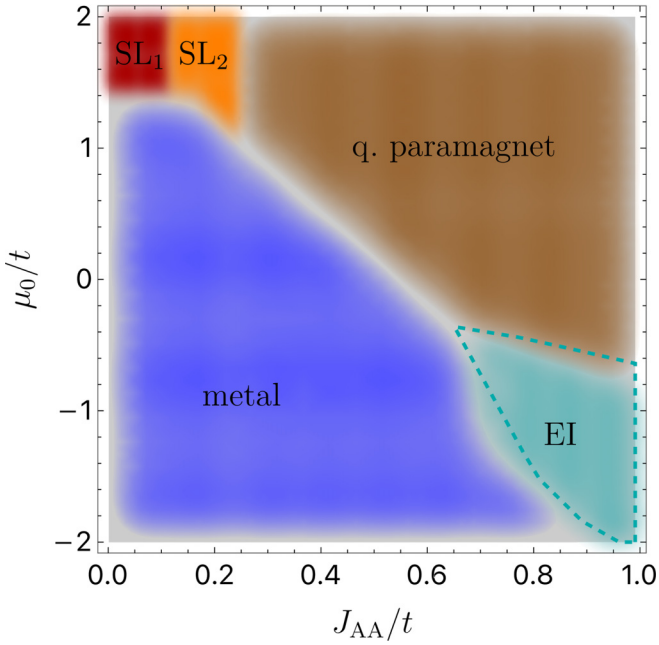

FIG. 3. The phase diagram for the hexagonal Mott insulator bilayer with the twist angle $\theta = 10^\circ$. The parameters used are $t_{AA} = t_{AB} = t/5$, $J = 0.5t$, $J_{AB} = 0.1t$, $J^{0}_{AA} = J^{0}_{AB} = 0.2t$, $J^{G}_{AA} = 0$. The blue dashed line indicates the change in the boundary of the EI phase when the twist angle is lowered to 7°.

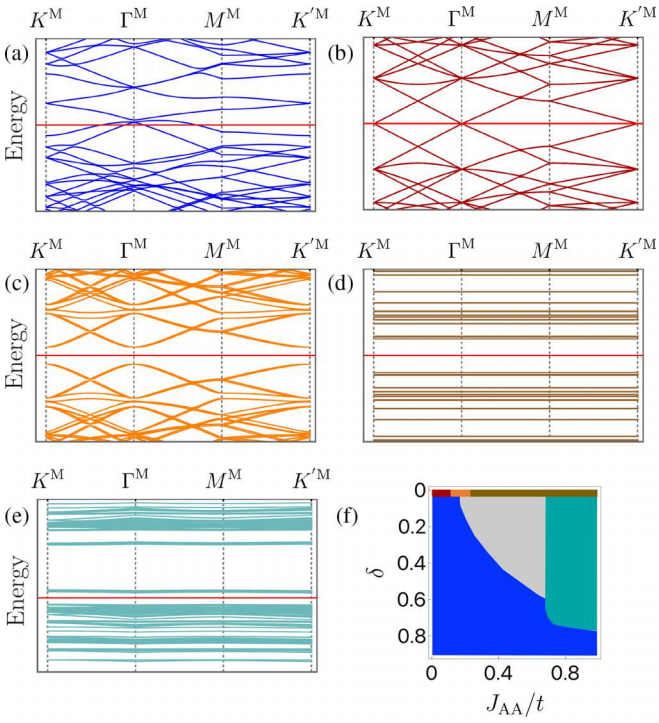

FIG. 4. (a)–(e) Examples of spinon band structure for all five phases in the phase diagram in Fig. 3, i.e., (a) metal, (b) $U(1) \times U(1)$ spin liquid, (c) $U(1)$ gapped spin liquid, (d) quantum paramagnet, and (e) excitonic insulator. The Fermi levels are shown with red lines. (f) Schematic phase diagram as a function of J_{AA} and the hole doping δ; gray color indicates the parameter region not attainable within the studied μ_0-J_{AA} values.

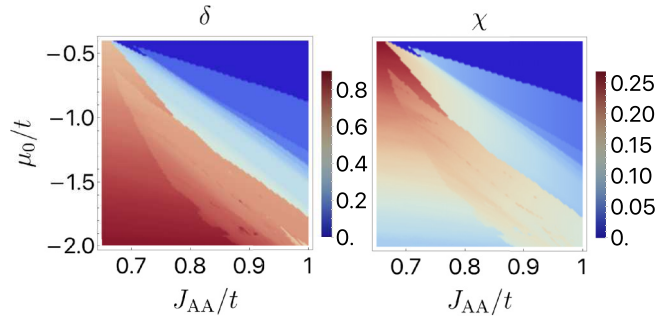

FIG. 5. Mean-field parameters δ and χ in the vicinity of the excitonic insulator phase in the bottom right corner of the phase diagram in Fig. 3. Both quantities experience abrupt changes as J_{AA} and μ_0 are varied when several minibands cross the Fermi level.

and symmetry properties is shown in Table I. Furthermore, the spinon band structures realized in each phase are shown in Fig. 4.

For small values of J_{AA}, the ground state corresponds to the uniform order parameter $\chi_{AA} = \chi_{BB}$, i.e., $\mathbf{q}^J = 0$. This *metallic* phase, highlighted in dark blue, exhibits a dispersion that is essentially a renormalized version of that found in twisted bilayer graphene. Yet there are key differences, such as the nonlinear behavior of the magic angle as a function of parameters, as discussed below.

For higher values of the chemical potential, μ_0, we obtain Mott insulating phases (i.e., no doping, $\delta = 0$). Within the parton mean-field theory, these phases are either the spin liquids or the quantum paramagnets. The spin liquid phases are highlighted in red and orange in the phase diagram: the first phase is the plain intralayer $U(1) \times U(1)$ *spin liquid* with $\chi \neq 0$ and all other order parameters being zero. The latter phase, highlighted with orange, is a $U(1)$ *spin liquid* state with the gap at $E = 0$ arising due to the development of the nontrivial interlayer spinon order parameter $\chi_{AA} = -\chi_{BB}$ with $\mathbf{q}^J_n = \mathbf{\Delta}_n$. Due to the gap opening, this phase features the chiral edge currents of spinons localized on the boundaries between the AB and BA stacking arrangements [33]. For larger values of interlayer Heisenberg exchange, J_{AA}, the Dirac kinetic term provided by the intralayer spinon order parameter vanishes, with the corresponding phase becoming a topologically trivial flat band. This gapped phase, which we call the *quantum paramagnet* and show with brown color, is characterized by the formation of interlayer singlets.

The last phase, shown with cyan, is insulating with $\delta > 0$ and is particularly distinctive compared to the noninteracting twisted models. The Fermi level in this phase lies between the minibands with the mean-field parameters δ and χ varying across the phase in a steplike fashion, as shown in Fig. 5. Thus, the latter phase encompasses multiple phases separated by the metal-insulator transitions. As one can infer from the Table I, in this phase, both the interlayer and intralayer spinon condensates are present. Furthermore, the combination of $\delta \neq 0$ and the momentum dependence of the order parameter breaks spontaneously the moiré translational symmetry, such that the area of the unit cell in the real space triples, as shown in Fig. 1(b). Therefore, this state is an exotic valence bond solid characterized by the formation of the interlayer singlets.

TABLE I. Summary of the phases. The first column labels the phase together with its color code in the diagram in Fig. 3. The next four columns represent the values of the parameters distinguishing the phases in the diagram. The sign "+" means that the order parameter is positive, and "−" stands for negative. The sixth column indicates whether the interlayer spinon order parameters $\chi_{AA(BB)}$ are uniform ($\mathbf{q}_n^J = 0$) or develop spatial modulation ($\mathbf{q}_n^J = \mathbf{\Delta}_n$). The last two columns show whether the C_2 symmetry protecting the Dirac cones and the moiré translations T_M are spontaneously broken (indicated by the cross mark) or preserved (shown with the check mark).

Phase	δ	χ	χ_{AA}	χ_{BB}	$\mathbf{q}_n^J$	C_2	T_M
[Red] $U(1) \times U(1)$ spin liquid	0	+	0	0	$\mathbf{\Delta}_n$	✓	✓
[Orange] $U(1)$ gapped spin liquid	0	+	+	−	$\mathbf{\Delta}_n$	✗	✓
[Brown] quantum paramagnet	0	0	+	−	$\mathbf{\Delta}_n$	✗	✓
[Blue] metal	+	+	+	+	0	✓	✓
[Cyan] excitonic insulator (EI)	+	+	+	−	$\mathbf{\Delta}_n$	✗	✗

This phase essentially represents the *excitonic insulator* (EI) of spinons, in analogy with the excitonic insulator arising due to pairing between an electron and a hole separated by a finite momentum vector [34]. In our case, it is a particle-hole bound state between the spinons belonging to different layers and separated by momentum $\mathbf{\Delta}_n$, which leads to the nonvanishing expectation value of the order parameters $\chi_{AA(BB)} = \langle \hat{f}^{(1)\dagger}_{A(B)} \hat{f}^{(2)}_{A(B)} \rangle$.

As indicated in Fig. 3 with the blue dashed line, the excitonic insulator phase expands toward $\mu_0 = 0$ as the twist angle is lowered due to the increase in the number of minibands. Therefore, at small twist angles, this phase is realized at a lower doping level. However, crucially, we find that the condition $J_{AA} \gg J^0_{AA}$ needs to be satisfied in order for the EI phase to exist; i.e., the superexchange at zero momentum should be much smaller than at the momentum $\mathbf{K}$. As a result, some destructive interference effects with respect to the nearest-neighbor superexchange are likely required to observe this phase. Lastly, we note that the mean-field parameters that distinguish different phases are the interlayer spinon susceptibilities χ_{AA} and χ_{BB}. The parameter χ_{AB} is found to be nonzero only in the metal phase.

Another distinctive aspect of the considered model is the superexchange dependence of the magic angles found in the correlated metallic phase. As discussed above, the Hamiltonian in this phase is in many ways analogous to the Bistritzer-MacDonald model, with certain parameters determined self-consistently. The magic angles then occur due to the interplay between the interactions and the dispersion, in turn, both dependent on mean-field parameters such as χ and δ.

In Fig. 6(a), we showcase the effect of the interlayer superexchanges J_{AA} and J_{AB} on the three largest magic angles. The main influence on the dispersion of the energy levels at neutrality can be captured via the renormalization of the effective intralayer and two interlayer tunneling terms

$$t^{\text{eff}} = \delta t + \frac{\chi J}{4},$$
$$t^{\text{eff}}_{AA} = \delta t_{AA} + \frac{\chi_{AA} J_{AA}}{4},$$
$$t^{\text{eff}}_{AB} = \delta t_{AB} + \frac{\chi_{AB} J_{AB}}{4}. \quad (18)$$

From Fig. 6(b), we infer that when the parameters J_{AA} and J_{AB} are increased, the ratios $t^{\text{eff}}_{AA}/t^{\text{eff}}$ and $t^{\text{eff}}_{AB}/t^{\text{eff}}$ also grow. This is to be expected from the definitions (18). However, the actual increase is faster than linear due to the mean-field renormalization of χ_{AA}, χ_{BB}, and χ_{AB}. Since the effective interlayer tunneling is increased, all magic angles increase in magnitude.

Next, we discuss the validity of our method. Large-N, slave-boson mean-field theory is a static approximation that becomes exact in the limit of $N \to \infty$ [35]. This naturally can raise the concern if our results can hold for $N = 2$. It is well established that the phase transition associated with the condensation of the slave boson is in general not a true phase transition and $1/N$ corrections can turn it into a crossover [35]. However, if the order parameter breaks additional symmetries such as translations or rotations, it is anticipated that the phase transition can survive [36]. We note that the excitonic insulator phase breaks moiré translational symmetry. In addition, for the single-band Hubbard model, slave-particle theories are

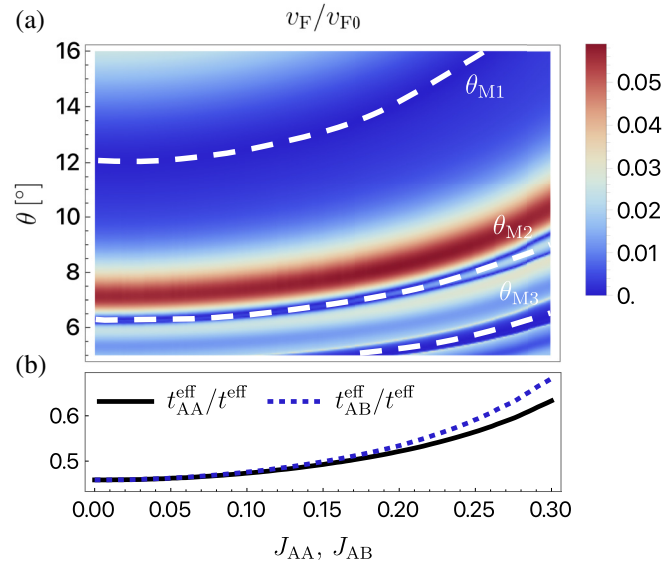

FIG. 6. Renormalization of the three largest magic angles of spinons (a) and the effective tunneling terms (b) as a function of parameters J_{AA} and J_{AB} as they are varied simultaneously. Due to the net increase in the interlayer tunneling with respect to the intralayer shown on the bottom panel, the magic angles increase as indicated on the Fermi velocity density plot on the top panel. The parameters used are $t_{AA} = t_{AB} = t/2$, $J = 0.2t$, $J^0_{AA} = J^0_{AB} = t/4$, and $J^G_{AA} = 0$, and $v_{F0} = 3at/2$ denotes the bare Fermi velocity.

benchmarked by quantum Monte Carlo [37] and dynamical mean field theory simulations [38], which show qualitative agreement [39].

IV. CONCLUSION

We examined the twisted hexagonal correlated insulators via the slave-boson mean-field theory. The associated phase diagram, which now results from the effect of twist on both the band structure and the form of interactions, is shown to host the exotic translational symmetry-breaking excitonic insulator phase. This phase arises due to the existence of the minigaps controlled by the interaction, and hence sensitive to the twist angle. Despite the similarity of our model Hamiltonian at the mean-field level to the Bistritzer-MacDonald model, the interactions play an essential role in the stabilization of phases that are absent in the noninteracting Bistritzer-MacDonald model. In particular, the flat bands corresponding to magic angles are determined by the electron-electron interactions as much as the tunneling terms between the layers. Furthermore, due to the correlated nature of underlying monolayers, changes in doping levels have a significant impact on the parameters of the model. The high tunability of the lower-dimensional materials with respect to doping raises hopes that the phenomenology described in this work can be observed in future experiments.

ACKNOWLEDGMENTS

We thank Arun Paramekanti and Liuyan Zhao for the fruitful discussions. P.G. acknowledges support from National Science Foundation Awards No. DMR-2130544 and No. DMR-2315063. This work was supported by the .S. Department of Energy, Office of Science, Office of Basic Energy Sciences, Material Sciences and Engineering Division, under Award No. DE-SC0025247. The work of I.K. is supported by the Julian Schwinger Foundation.

APPENDIX A: MEAN-FIELD THEORY FOR AA-STACKING PATTERN

In this Appendix, we derive the mean-field formalism for the AA-stacked bilayer. We assume the interlayer hopping is local and the AB hopping is absent. In the limit of $U \to \infty$ and close to half filling, the t-J model is a valid approximation,

$$\hat{H}_{t-J} = -\sum_{\langle ij\rangle} t_{ij}\hat{P}\hat{c}^{\dagger}_{i\sigma}\hat{c}_{j\sigma}\hat{P} - \mu_0\sum_i \hat{c}^{\dagger}_{i\sigma}\hat{c}_{i\sigma} + \sum_{\langle ij\rangle} J_{ij}\left(\hat{\mathbf{S}}_i\cdot\hat{\mathbf{S}}_j - \frac{1}{4}\hat{n}_i\hat{n}_j\right), \tag{A1}$$

where t_{ij} denotes the hopping between the sites i and j (both of the indices may take values in the first and the second layers), J_{ij} is the superexchange parameter, and $\hat{P}$ is the projector into the space of singly occupied sites. The operators $\hat{c}_{i\sigma}$ and $\hat{c}^{\dagger}_{i\sigma}$ are the annihilation and creation operators of fermions with position i and spin σ. In order to accommodate the constraint of not having doubly occupied sites, we use the parton decomposition, $\hat{c}_{i\sigma} = \hat{b}^{\dagger}_i\hat{f}_{i\sigma}$. The constraint takes the convenient for numerical calculations holonomic form $\sum_\sigma \hat{f}^{\dagger}_{i\sigma}\hat{f}_{i\sigma} + \hat{b}^{\dagger}_i\hat{b}_i = 1$.

In terms of the parton fields, the t-J model Hamiltonian (A1) with the added constraint reads [6]

$$\hat{H}_0 = -t\sum_{\langle ij\rangle}(\hat{f}^{\dagger}_{i\sigma}\hat{f}_{j\sigma}\hat{b}_i\hat{b}^{\dagger}_j + \text{c.c.}) - \mu_0\sum_i \hat{f}^{\dagger}_{i\sigma}\hat{f}_{i\sigma} + J\sum_{\langle ij\rangle}\left(\hat{\mathbf{S}}_i\cdot\hat{\mathbf{S}}_j - \frac{1}{4}\hat{n}_i\hat{n}_j\right) + \lambda\sum_i(\hat{f}^{\dagger}_{i\sigma}\hat{f}_{i\sigma} + \hat{b}^{\dagger}_i\hat{b}_i - 1). \tag{A2}$$

We assume constant mean occupation of holes $\langle\hat{b}^{\dagger}_i\hat{b}_i\rangle = \delta$ and decouple the spinon terms in the exchange channel, introducing the real-valued Hubbard-Stratonovich field $\chi_{ij} = \langle\hat{f}^{\dagger}_{i\sigma}\hat{f}_{j\sigma}\rangle\,\delta_{\langle ij\rangle}$ that modifies the nearest-neighbor hoppings. The mean-field expressions for the density-density and spin-spin terms then read

$$\begin{aligned}\hat{n}_i\hat{n}_j &= (1-\hat{b}^{\dagger}_i\hat{b}_i)(1-\hat{b}^{\dagger}_j\hat{b}_j) \sim (1-\delta)^2,\\ \hat{\mathbf{S}}_i\cdot\hat{\mathbf{S}}_j &= 2\hat{f}^{\dagger}_{i\sigma}\hat{f}_{i\beta}\hat{f}^{\dagger}_{j\beta}\hat{f}_{j\sigma} - (\hat{f}^{\dagger}_{i\sigma}\hat{f}_{i\sigma})(\hat{f}^{\dagger}_{j\beta}f_{j\beta})\\ &\sim \tfrac{1}{4}\chi^2_{ij} - \tfrac{1}{4}(\chi_{ij}f^{\dagger}_{\sigma i}f_{\sigma j} + \text{c.c.}) + \tfrac{1}{4}(1-\delta).\end{aligned} \tag{A3}$$

The proof of the last identity is contained in Sec. A 1. By utilizing the identities (A3) in (A2) and taking the Fourier transform, we obtain the Hamiltonian for a single monolayer

$$\hat{H}_0 = -\left(\delta t + \frac{J\chi}{4}\right)\sum_{\mathbf{k}\sigma}[g(\mathbf{k})\hat{f}^{\dagger}_{\mathbf{k}\sigma\mathrm{A}}\hat{f}_{\mathbf{k}\sigma\mathrm{B}} + \text{c.c.}] + (\lambda-\mu_0)\sum_{\mathbf{k}\sigma\alpha}\hat{f}^{\dagger}_{\mathbf{k}\sigma\alpha}\hat{f}_{\mathbf{k}\sigma\alpha} + \frac{3JN}{4}\chi^2 + \frac{N}{4}(1-\delta)(3\delta J - 8\lambda), \tag{A4}$$

where N is the number of unit cells, and the function $g(\mathbf{k}) = \sum_j e^{-i\mathbf{k}\cdot\boldsymbol{\gamma}_j}$ is the hopping term well known from the theory of the graphene monolayer: in our notations $\boldsymbol{\gamma}_1 = (0, a)$ with the remaining $\boldsymbol{\gamma}_j$ obtained by $2\pi/3$ rotations. In order to describe a strongly interacting bilayer, we take the Hamiltonian (A4) twice—for the layers 1 and 2—and supplement the sum by the interlayer hopping and interlayer superexchange

$$\hat{H}_{\mathrm{AA}} = \hat{H}^{(1)}_0 + \hat{H}^{(2)}_0 + \hat{H}_t + \hat{H}_J, \tag{A5}$$

where in the basis

$$\hat{f}_{\mathbf{k}} = \left(\hat{f}^{(1)}_{\mathbf{k}A}\ \hat{f}^{(1)}_{\mathbf{k}B}\ \hat{f}^{(2)}_{\mathbf{k}A}\ \hat{f}^{(2)}_{\mathbf{k}B}\right) \tag{A6}$$

we write

$$H_t = -\begin{pmatrix} 0 & 0 & 3\delta t_{\mathrm{AA}} & 0\\ 0 & 0 & 0 & 3\delta t_{\mathrm{AA}}\\ 3\delta t_{\mathrm{AA}} & 0 & 0 & 0\\ 0 & 3\delta t_{\mathrm{AA}} & 0 & 0\end{pmatrix}, \tag{A7}$$

with the hopping $t_{\rm AA}$ tripled to make the comparison with the nonzero twist angle case more convenient. We use $3J_{\rm AA}$ for the superexchange alike. The interlayer superexchange contains spin-spin and density-density interlayer terms,

$$\hat{H}_J = 3J_{\rm AA}\sum_i \left(\hat{\mathbf{S}}^{(1)}_{i\rm A}\cdot\hat{\mathbf{S}}^{(2)}_{i\rm A} + \hat{\mathbf{S}}^{(1)}_{i\rm B}\cdot\hat{\mathbf{S}}^{(2)}_{i\rm B}\right) - 3J_{\rm AA}\sum_i\left(\frac{1}{4}\hat{n}^{(1)}_{i\rm A}\hat{n}^{(2)}_{i\rm A} - \frac{1}{4}\hat{n}^{(1)}_{i\rm B}\hat{n}^{(2)}_{i\rm B}\right). \tag{A8}$$

Making a further assumption that the hole occupation is the same in each layer and sublattice, all the above terms can be treated using the expressions analogous to (A3). The resulting Hamiltonian for the AA stacking reads

$$\hat{H}_{\rm untw} = -\sum_{\mathbf{k}\sigma}\hat{f}^\dagger_{\mathbf{k}\sigma}\begin{pmatrix} \mu_0-\lambda & \left(\delta t+\frac{\chi J}{4}\right)g(\mathbf{k}) & 3\delta t_{\rm AA}+\frac{3\chi_{\rm AA}J_{\rm AA}}{4} & 0\\ \left(\delta t+\frac{\chi J}{4}\right)g^*(\mathbf{k}) & \mu_0-\lambda & 0 & 3\delta t_{\rm AA}+\frac{3\chi_{\rm BB}J_{\rm AA}}{4}\\ 3\delta t_{\rm AA}+\frac{3\chi_{\rm AA}J_{\rm AA}}{4} & 0 & \mu_0-\lambda & \left(\delta t+\frac{\chi J}{4}\right)g(\mathbf{k})\\ 0 & 3\delta t_{\rm AA}+\frac{3\chi_{\rm BB}J_{\rm AA}}{4} & \left(\delta t+\frac{\chi J}{4}\right)g^*(\mathbf{k}) & \mu_0-\lambda \end{pmatrix}\hat{f}_{\mathbf{k}\sigma} + H_{\rm const}, \tag{A9}$$

where the constant term is $H_{\rm const} = \frac{3}{2}NJ\chi^2 + \frac{3NJ_{\rm AA}}{4}(\chi^2_{\rm AA}+\chi^2_{\rm BB}) + \frac{N}{2}(1-\delta)(3\delta J + 3\delta J_{\rm AA} - 8\lambda)$. The parameters of the Hamiltonian are μ_0, the intra- and interlayer hoppings t and $t_{\rm AA}$, and the intra- and interlayer superexchanges J and $J_{\rm AA}$. The mean-field parameters χ, χ_A, χ_B, λ, and δ are self-consistently determined by minimizing the free energy,

$$\begin{aligned}
\chi &= \frac{1}{6}\int_{\rm BZ}\frac{d^2\mathbf{k}}{K}\sum_{n=1}^{4}\langle n\mathbf{k}|\hat{H}_0|n\mathbf{k}\rangle\,\theta(E_F - E_n(\mathbf{k})) \equiv \frac{I_0}{6},\\
\chi_{\rm AA(BB)} &= \int_{\rm BZ}\frac{d^2\mathbf{k}}{K}\sum_{n=1}^{4}\langle n\mathbf{k}|\hat{H}_{\rm AA(BB)}|n\mathbf{k}\rangle\,\theta(E_F - E_n(\mathbf{k})) \equiv I_{\rm AA(BB)},\\
\delta &= 1 - \frac{1}{2}\int_{\rm BZ}\frac{d^2\mathbf{k}}{K}\sum_{n=1}^{4}\theta(E_F - E_n(\mathbf{k})),\\
\lambda &= \frac{1}{2}tI_0 + \frac{3t_{\rm AA}}{2}(I_{\rm AA}+I_{\rm BB}) - \frac{3}{8}(1-2\delta)(J+J_{\rm AA}),
\end{aligned} \tag{A10}$$

where $\hat{H}_0 = \sum_{\mathbf{k}l} g(\mathbf{k})\hat{f}^{(l)\dagger}_{\mathbf{k}\rm A}\hat{f}^{(l)}_{\mathbf{k}\rm B} + \text{H.c.}$, $\hat{H}_{\rm AA(BB)} = \sum_{\mathbf{k}}\hat{f}^{(1)\dagger}_{\mathbf{k}\rm A(B)}\hat{f}^{(2)}_{\mathbf{k}\rm A(B)} + \text{H.c.}$, $E_n(\mathbf{k})$ and $|n\mathbf{k}\rangle$ are the eigenvalues and eigenvectors of $\hat{H}_{\rm untw}$, K is the area of the hexagonal Brillouin zone, and θ denotes a step function.

Mean-field treatment of $\hat{\mathbf{S}}_i\cdot\hat{\mathbf{S}}_j$ term

We start by recalling the identity for Pauli matrices $\sigma_{\alpha\beta}\sigma_{\gamma\delta} = 2\delta_{\alpha\delta}\delta_{\beta\gamma} - \delta_{\alpha\beta}\delta_{\gamma\delta}$. With this, the spin exchange can be cast as

$$4(\hat{\mathbf{S}}_i\cdot\hat{\mathbf{S}}_j) = 2\hat{f}^\dagger_{\sigma_i}\hat{f}_{\beta i}\hat{f}^\dagger_{\beta j}\hat{f}_{\sigma j} - \hat{f}^\dagger_{\sigma_i}\hat{f}_{\sigma_i}\hat{f}^\dagger_{\beta j}\hat{f}_{\beta j}. \tag{A11}$$

The first term on the right-hand side we write as

$$2\hat{f}^\dagger_{\sigma i}\hat{f}_{\sigma j}\hat{f}_{\beta i}\hat{f}^\dagger_{\beta j} + 2\hat{n}_i = -2\hat{f}^\dagger_{\sigma i}\hat{f}_{\sigma j}\hat{f}^\dagger_{\beta j}\hat{f}_{\beta i} + 2\hat{n}_i. \tag{A12}$$

The remaining term is expanded as

$$\begin{aligned}
&\hat{f}^\dagger_{\uparrow i}\hat{f}_{\uparrow i}\hat{f}^\dagger_{\uparrow j}\hat{f}_{\uparrow j} + \hat{f}^\dagger_{\downarrow i}\hat{f}_{\downarrow i}\hat{f}^\dagger_{\downarrow j}\hat{f}_{\downarrow j}\\
&- \hat{f}^\dagger_{\uparrow i}\hat{f}_{\uparrow j}\hat{f}^\dagger_{\downarrow j}\hat{f}_{\downarrow i} - \hat{f}^\dagger_{\downarrow i}\hat{f}_{\downarrow j}\hat{f}^\dagger_{\uparrow j}\hat{f}_{\uparrow i}\\
&+ \hat{f}^\dagger_{\uparrow i}\hat{f}_{\uparrow j}\hat{f}^\dagger_{\downarrow j}\hat{f}_{\downarrow i} + \hat{f}^\dagger_{\downarrow i}\hat{f}_{\downarrow j}\hat{f}^\dagger_{\uparrow j}\hat{f}_{\uparrow i}\\
&+ \hat{f}^\dagger_{\uparrow i}\hat{f}_{\uparrow i}\hat{f}^\dagger_{\downarrow j}\hat{f}_{\downarrow j} + \hat{f}^\dagger_{\downarrow i}\hat{f}_{\downarrow i}\hat{f}^\dagger_{\uparrow j}\hat{f}_{\uparrow j},
\end{aligned} \tag{A13}$$

where in the second line we added and in the third line removed the same two terms. Using the anticommutation relations, $\{\hat{f}^\dagger_{i\alpha}, \hat{f}_{j\beta}\} = \delta_{ij}\delta_{\alpha\beta}$, we move all the operators with a dagger in the last two lines to the left, which gives overall

$$\begin{aligned}
4(\hat{\mathbf{S}}_i\cdot\hat{\mathbf{S}}_j) = \hat{n}_{i\uparrow} + \hat{n}_{i\downarrow} &- \hat{f}^\dagger_{\sigma_i}\hat{f}_{\sigma j}\hat{f}^\dagger_{\beta j}\hat{f}_{\beta i} - \hat{f}^\dagger_{\uparrow i}\hat{f}^\dagger_{\downarrow j}\hat{f}_{\uparrow j}\hat{f}_{\downarrow i}\\
&- \hat{f}^\dagger_{\downarrow i}\hat{f}^\dagger_{\uparrow j}\hat{f}_{\downarrow j}\hat{f}_{\uparrow i} + \hat{f}^\dagger_{\uparrow i}\hat{f}^\dagger_{\downarrow j}\hat{f}_{\downarrow j}\hat{f}_{\uparrow i}\\
&+ \hat{f}^\dagger_{\downarrow i}\hat{f}^\dagger_{\uparrow j}\hat{f}_{\uparrow j}\hat{f}_{\downarrow i}.
\end{aligned} \tag{A14}$$

The last four terms combine into the pairing term $(\hat{f}^\dagger_{\uparrow i}\hat{f}^\dagger_{\downarrow j} - \hat{f}^\dagger_{\downarrow i}\hat{f}^\dagger_{\uparrow j})(\hat{f}_{\downarrow j}\hat{f}_{\uparrow i} - \hat{f}_{\uparrow j}\hat{f}_{\downarrow i})$ that we ignore in this work. Thus, we obtain the final expression $\hat{\mathbf{S}}_i\cdot\hat{\mathbf{S}}_j \simeq -\frac{1}{4}\hat{f}^\dagger_{\alpha i}\hat{f}_{\alpha j}\hat{f}^\dagger_{\beta j}\hat{f}_{\beta i} + \frac{1}{4}\hat{n}_i \sim -\chi_{ij}\hat{f}^\dagger_{\beta j}\hat{f}_{\beta i} - \chi_{ij}\hat{f}^\dagger_{\beta i}\hat{f}_{\beta j} + \chi^2_{ij} + \frac{1}{4}\hat{n}_i$.

APPENDIX B: DERIVATION OF THE TWISTED BILAYER MEAN-FIELD HAMILTONIAN

In this Appendix, we derive the effective continuous model of the twisted strongly correlated bilayer. In the limit of zero twist angle, we expect it to reproduce the continuum limit of the Hamiltonian (A9).

We use the indices $a, b = 1, 2$ to denote the layer index, and $\alpha, \beta = \rm A, B$ to label sublattices. The layers 1 and 2 are rotated by the angles $\theta/2$ and $-\theta/2$ with respect to an imaginary reference layer. The reciprocal lattice vectors in the reference layer are given by $\mathbf{G}_{1,2} = 2\pi/(\sqrt{3}a)(-1, \mp 1/\sqrt{3})$. The moiré reciprocal lattice vectors in the small twist angle limit are $\mathbf{G}^{\rm M}_{1,2} = 2\pi/(\sqrt{3}a)(\pm 1/\sqrt{3}, -1)\theta$ (we assume throughout

that θ is small). The vectors $\mathbf{\Delta}_n$ connect nearest neighbors in the moiré lattice, with $\mathbf{\Delta}_1 = (0, 4\pi\theta/(3\sqrt{3}a))$, and $\mathbf{\Delta}_{2,3}$ obtained from it by $2\pi/3$ and $4\pi/3$ clockwise rotations (see the left panel in Fig. 2). The moiré reciprocal lattice vectors $\mathbf{G}^{\mathrm{M}}$ and $\mathbf{\Delta}_n$ are related as

$$\mathbf{G}_1^{\mathrm{M}} = \mathbf{\Delta}_2 - \mathbf{\Delta}_1, \quad \mathbf{G}_2^{\mathrm{M}} = \mathbf{\Delta}_3 - \mathbf{\Delta}_1. \tag{B1}$$

The derivation below closely follows one of the original continuous Bistritzer-MacDonald (BM) model [40]. The starting assumption is that one can write the t-J model (A1) in the Wannier basis of the original monolayers. The form of the interlayer terms in the resulting parton mean-field theory will essentially depend on the properties of the interlayer superexchange parameter $J(|i-j|)$. It is clear that if the layers are sufficiently far away from each other, the layer corrugation is smooth, and the spatial variation of J is also expected to be smooth. With this assumption, a BM-type model can be derived, as we demonstrate below.

After switching from fermion to spinon fields and introducing the mean-field parameter χ_{ij} as explained in Appendix A, one obtains a mean-field Hamiltonian analogous to (A9). The essential difference is that in the nonzero twist angle case, the superexchange is no longer constant in space, which leads to the appearance of the terms

$$\hat{U} = -\frac{1}{4}\sum_{ij} J(|i-j|)\chi_{ij}\hat{f}_i^{\dagger(1)}\hat{f}_j^{(2)},$$

$$\hat{U}^* = -\frac{1}{4}\sum_{ij} J(|i-j|)\chi_{ij}^*\hat{f}_j^{\dagger(1)}\hat{f}_i^{(2)},$$

$$X = \frac{1}{4}\sum_{ij} J(|i-j|)\chi_{ij}^*\chi_{ij},$$

$$\mathcal{N} = -\frac{1}{4}\sum_{ij} J(|i-j|)\hat{n}_i\hat{n}_j, \tag{B2}$$

in place of the superexchange terms in (A9). We further assume that the mean field χ_{ij} can condense at nonzero momenta $\mathbf{q}_n^J$,

$$\chi_{ij} = \chi_{\alpha\beta}\sum_{n=1}^{3} e^{i\mathbf{\Delta}_n\cdot\mathbf{j}}. \tag{B3}$$

The reason to expect $\mathbf{q}_n^J \neq 0$ is that when the interlayer superexchange is sufficiently high, the gap opening is energetically favorable. In order for the gap to open, the Dirac cones belonging to different layers need to be able to hybridize at zero momentum. This is achieved precisely by setting $\mathbf{q}_n^J = \mathbf{\Delta}_n$, which will be evident from the form of the Hamiltonian obtained below.

We begin our BM-type model derivation by evaluating the expectation value of the first ($\hat{U}$) term in (B2) between the monolayer Bloch states,

$$\left|f_{\mathbf{p}\alpha}^{(a)}\right\rangle = \frac{1}{\sqrt{N}}\sum_{\mathbf{R}^{(a)}} e^{i\mathbf{p}\cdot(\mathbf{R}^{(a)}+\mathbf{t}_\alpha^{(a)})}\left|\mathbf{R}^{(a)}+\mathbf{t}_\alpha^{(a)}\right\rangle, \tag{B4}$$

where $\mathbf{R}^{(a)}$ labels the positions of atoms on the A sublattice in layer (a), and $\mathbf{t}_\alpha^{(a)}$ is the basis vector in the same layer: $\mathbf{t}_{\mathrm{A}} = (0,0)$, $\mathbf{t}_{\mathrm{B}} = (a,0)$ before twisting. The requisite interlayer matrix element can be written as

$$U_{\alpha\beta}^{(12)}(\mathbf{p},\mathbf{p}') \equiv \left\langle f_{\mathbf{p}\alpha}^{(1)}\middle|\hat{U}\middle|f_{\mathbf{p}'\beta}^{(2)}\right\rangle = -\frac{\chi_{\alpha\beta}}{4N}\sum_{\mathbf{R}^{(1)}\mathbf{R}^{(2)}n} e^{-i\mathbf{p}\cdot(\mathbf{R}^{(1)}+\mathbf{t}_\alpha^{(1)})}e^{i\mathbf{p}'\cdot(\mathbf{R}^{(2)}+\mathbf{t}_\beta^{(2)})}e^{i\mathbf{q}_n^J\cdot(\mathbf{R}^{(2)}+\mathbf{t}_\beta^{(2)})}J\left(\mathbf{R}^{(1)}+\mathbf{t}_\alpha^{(1)}-\mathbf{R}^{(2)}-\mathbf{t}_\beta^{(2)}\right). \tag{B5}$$

We further expand J in a Fourier integral

$$J\left(\mathbf{R}^{(1)}+\mathbf{t}_\alpha^{(1)}-\mathbf{R}^{(2)}-\mathbf{t}_\beta^{(2)}\right) = \frac{1}{N\Omega}\sum_{\mathbf{q}}\sum_{\mathbf{G}} J_{\mathbf{q}+\mathbf{G}}^{(12)}e^{i(\mathbf{q}+\mathbf{G})\cdot(\mathbf{R}^{(1)}+\mathbf{t}_\alpha^{(1)}-\mathbf{R}^{(2)}-\mathbf{t}_\beta^{(2)})}, \tag{B6}$$

where the $\mathbf{G}$ summation runs over the reciprocal lattice vectors of the reference layer, and $\mathbf{q}$ summation is over the hexagonal Brillouin zone. The letter Ω denotes the size of the unit cell in the real space, and N is the number of electrons. Plugging this expression back into the matrix element (B5) produces

$$U_{\alpha\beta}^{(12)}(\mathbf{p},\mathbf{p}') = -\frac{\chi_{\alpha\beta}}{4N^2\Omega}\sum_{\mathbf{R}^{(1)}\mathbf{R}^{(2)}}\sum_{\mathbf{q}\mathbf{G}n} e^{i(\mathbf{q}+\mathbf{G}-\mathbf{p})\cdot\mathbf{R}^{(1)}}e^{-i(\mathbf{q}+\mathbf{G}-\mathbf{p}'-\mathbf{q}_n^J)\cdot\mathbf{R}^{(2)}}J_{\mathbf{q}+\mathbf{G}}^{(12)}e^{i(\mathbf{q}_n^J\cdot\mathbf{t}_\beta^{(2)}+\mathbf{p}'\cdot\mathbf{t}_\beta^{(2)}-\mathbf{p}\cdot\mathbf{t}_\alpha^{(1)}+\mathbf{q}\cdot(\mathbf{t}_\alpha^{(1)}-\mathbf{t}_\beta^{(2)})+\mathbf{G}\cdot(\mathbf{t}_\alpha^{(1)}-\mathbf{t}_\beta^{(2)}))}. \tag{B7}$$

We further make use of the identities

$$\frac{1}{N}\sum_{\mathbf{R}^{(2)}} e^{i(\mathbf{q}+\mathbf{G}-\mathbf{p}'-\mathbf{q}_n^J)\cdot\mathbf{R}^{(2)}} = \sum_{\mathbf{G}^{(2)}}\delta_{\mathbf{q}+\mathbf{G},\mathbf{p}'+\mathbf{q}_n^J+\mathbf{G}^{(2)}} = \sum_{\mathbf{G}'}\delta_{\mathbf{p}'-\mathbf{q}-\mathbf{G}+R_-\mathbf{G}',-\mathbf{q}_n^J},$$

$$\frac{1}{N}\sum_{\mathbf{R}^{(1)}} e^{i(\mathbf{q}+\mathbf{G}-\mathbf{p})\cdot\mathbf{R}^{(1)}} = \sum_{\mathbf{G}''}\delta_{\mathbf{p}-\mathbf{q}-\mathbf{G}+R_+\mathbf{G}'',0}, \tag{B8}$$

where $\mathbf{G}'$ and $\mathbf{G}''$ lie within the reference layer, R_+ is a rotation matrix with parameter $\theta/2$, and $R_- = R_+^T$. Integration over $\mathbf{q}$ present in (B7) combines these two delta functions into the one with the argument

$$\mathbf{p}-\mathbf{p}'+R_+\mathbf{G}''-R_-\mathbf{G}'-\mathbf{q}_n^J \tag{B9}$$

with a condition $\mathbf{q} = \mathbf{p}'-\mathbf{G}+R_-\mathbf{G}'+\mathbf{q}_n^J$. Substituting these in (B7) gives

$$U_{\alpha\beta}^{(12)}(\mathbf{p},\mathbf{p}') = -\frac{\chi_{\alpha\beta}}{4\Omega}\sum_{\mathbf{G}\mathbf{G}'\mathbf{G}''n} J_{\mathbf{p}'+R_-\mathbf{G}'+\mathbf{q}_n^J}^{(12)}\delta_{\mathbf{p}-\mathbf{p}'+R_+\mathbf{G}''-R_-\mathbf{G}'-\mathbf{q}_n^J}e^{i\kappa}, \tag{B10}$$

where the phase is

$$\begin{aligned}\kappa &= \mathbf{p}'\cdot\mathbf{t}_\beta^{(2)} - \mathbf{p}\cdot\mathbf{t}_\alpha^{(1)} + \left(\mathbf{t}_\alpha^{(1)} - \mathbf{t}_\beta^{(2)}\right)\cdot(\mathbf{p}' + R_-\mathbf{G}') + \mathbf{q}_n^J\cdot\mathbf{t}_\alpha^{(1)} \\ &= -\mathbf{p}\cdot\mathbf{t}_\alpha^{(1)} + \mathbf{p}'\cdot\mathbf{t}_\alpha^{(1)} + \left(\mathbf{p} - \mathbf{p}' + R_+\mathbf{G}'' - \mathbf{q}_n^J\right)\cdot\mathbf{t}_\alpha^{(1)} - R_-\mathbf{G}'\cdot\mathbf{t}_\beta^{(2)} + \mathbf{q}_n^J\cdot\mathbf{t}_\alpha^{(1)} \\ &= R_+\mathbf{G}''\cdot\mathbf{t}_\alpha^{(1)} - R_-\mathbf{G}'\cdot\mathbf{t}_\beta^{(2)}. \end{aligned} \tag{B11}$$

The matrix element then takes the form

$$U_{\alpha\beta}^{(12)}(\mathbf{p},\mathbf{p}') = -\frac{\chi_{\alpha\beta}}{4\Omega}\sum_{\mathbf{G}'\mathbf{G}''n} J^{(12)}_{\mathbf{p}'+R_-\mathbf{G}'+\mathbf{q}_n^J}\delta_{\mathbf{p}-\mathbf{p}'+R_+\mathbf{G}''-R_-\mathbf{G}'-\mathbf{q}_n^J} e^{i(R_+\mathbf{G}''\cdot\mathbf{t}_\alpha^{(1)} - R_-\mathbf{G}'\cdot\mathbf{t}_\beta^{(2)})}. \tag{B12}$$

In the above form, we make a series of approximations. First, we expand around the momenta in the vicinity of the K point in both layers,

$$\mathbf{p} = R_+K + \delta\mathbf{p}, \quad \mathbf{p}' = R_-K + \delta\mathbf{p}'. \tag{B13}$$

As J decays fast in the momentum space away from the rotated layer K points R_+K, R_+C_3K, and $R_+C_3^2K$, we keep only $\mathbf{G}_1' = 0$, $\mathbf{G}_2' = C_3K - K$, and $\mathbf{G}_3' = C_3^2K - K$. For sufficiently small twist angles, the delta function imposes alike $\mathbf{G}_1'' = 0$, $\mathbf{G}_2'' = C_3K - K$, and $\mathbf{G}_3'' = C_3^2K - K$. Since we assume $\mathbf{q}_n^J \ll \mathbf{G}'$, we can let

$$J^{(12)}_{\mathbf{p}'+R_+\mathbf{G}'+\mathbf{q}_n^J} \simeq J^{(12)}_{\mathbf{p}'+R_+\mathbf{G}'} \simeq \Omega J_{\mathrm{AA}}\delta_{\alpha\beta} + \Omega J_{\mathrm{AB}}(1-\delta_{\alpha\beta}), \tag{B14}$$

where we used the requirements imposed by a C_3 symmetry. We further introduce the moiré reciprocal lattice vectors that assume constant value in the small-angle approximation,

$$R_+\mathbf{G}_1' - R_-\mathbf{G}_1'' = 0, \quad R_+\mathbf{G}_2' - R_-\mathbf{G}_2'' \equiv \mathbf{G}_1^{\mathrm{M}}, \quad R_+\mathbf{G}_3' - R_-\mathbf{G}_3'' \equiv \mathbf{G}_1^{\mathrm{M}} + \mathbf{G}_2^{\mathrm{M}}. \tag{B15}$$

The final form of this interlayer superexchange is then

$$\begin{aligned} U^{(12)}_{\delta\mathbf{p}\delta\mathbf{p}'} = &-\frac{1}{4}\sum_n \begin{pmatrix} \chi_{AA}J_{\mathrm{AA}} & \chi_{AB}J_{\mathrm{AB}} \\ \chi_{AB}J_{\mathrm{AB}} & \chi_{BB}J_{\mathrm{AA}}\end{pmatrix}\delta_{\delta\mathbf{p}+\boldsymbol{\Delta}_1-\mathbf{q}_n^J,\delta\mathbf{p}'} - \frac{1}{4}\sum_n \begin{pmatrix} \chi_{AA}J_{\mathrm{AA}} & \omega\chi_{AB}J_{\mathrm{AB}} \\ \omega^{-1}\chi_{AB}J_{\mathrm{AB}} & \chi_{BB}J_{\mathrm{AA}}\end{pmatrix}\delta_{\delta\mathbf{p}+\boldsymbol{\Delta}_2-\mathbf{q}_n^J,\delta\mathbf{p}'} \\ &-\frac{1}{4}\sum_n \begin{pmatrix} \chi_{AA}J_{\mathrm{AA}} & \omega^{-1}\chi_{AB}J_{\mathrm{AB}} \\ \omega\chi_{AB}J_{\mathrm{AB}} & \chi_{BB}J_{\mathrm{AA}}\end{pmatrix}\delta_{\delta\mathbf{p}+\boldsymbol{\Delta}_3-\mathbf{q}_n^J,\delta\mathbf{p}'}, \end{aligned} \tag{B16}$$

where $\omega = e^{2\pi i/3}$. If we set $\mathbf{q}_n^J = \boldsymbol{\Delta}_n$, unlike in the classic BM model, the next-nearest neighbors on the moiré lattice can also hybridize as shown with the long black arrows in Fig. 2(b). Hybridization at zero momentum also becomes possible.

We now discuss the Fourier transform of the X term in (B2). It is convenient to perform this calculation separately for the $\mathbf{q}_n^J = 0$ and $\mathbf{q}_n^J = \boldsymbol{\Delta}_n$ cases. We begin with the first case:

$$\frac{\chi_{\alpha\beta}^2}{4}\sum_{ij}J(|i-j|) = \frac{\chi_{\alpha\beta}^2}{4\Omega N}\sum_{\mathbf{R}^{(1)}\mathbf{R}^{(2)}\mathbf{G}\mathbf{q}} J_{\mathbf{G}+\mathbf{q}}e^{i(\mathbf{G}+\mathbf{q})\cdot(\mathbf{R}^{(1)}-\mathbf{R}^{(2)}+\mathbf{t}^{(1)}-\mathbf{t}^{(2)})} = \frac{N\chi_{\alpha\beta}^2}{4\Omega}\sum_{\mathbf{G}^{(1)}\mathbf{G}^{(2)}\mathbf{G}\mathbf{q}} J_{\mathbf{G}+\mathbf{q}}\delta_{\mathbf{G}+\mathbf{q},\mathbf{G}^{(1)}}\delta_{\mathbf{G}+\mathbf{q},\mathbf{G}^{(2)}}e^{i\mathbf{G}^{(1)}\cdot(\mathbf{t}^{(1)}-\mathbf{t}^{(2)})}. \tag{B17}$$

At nonzero twist, the only matching reciprocal lattice vectors are $\mathbf{G}^{(1)} = 0$ and $\mathbf{G}^{(2)} = 0$, so we obtain

$$\frac{N\chi_{\alpha\beta}^2}{4\Omega}\sum_{\mathbf{G}\mathbf{q}} J_{\mathbf{G}+\mathbf{q}}\delta_{\mathbf{G}+\mathbf{q},0} = \frac{N\chi_{\alpha\beta}^2}{4}J^{\mathbf{0}}, \tag{B18}$$

where we introduced $J_{\mathbf{k}=0} = \Omega J^{\mathbf{0}}$. An analogous calculation for the $\mathbf{q}_n^J = \boldsymbol{\Delta}_n$ case proceeds as follows:

$$\begin{aligned}\frac{\chi_{\alpha\beta}^2}{4}\sum_{ijnn'}J(|i-j|)e^{-i(\boldsymbol{\Delta}_{n'}-\boldsymbol{\Delta}_n)\cdot j} &= \frac{\chi_{\alpha\beta}^2}{4\Omega N}\sum_{\mathbf{R}^{(1)}\mathbf{R}^{(2)}\mathbf{G}\mathbf{q}nn'} J_{\mathbf{G}+\mathbf{q}}e^{i(\mathbf{G}+\mathbf{q})\cdot(\mathbf{R}^{(1)}-\mathbf{R}^{(2)}+\mathbf{t}^{(1)}-\mathbf{t}^{(2)})}e^{-i(\boldsymbol{\Delta}_{n'}-\boldsymbol{\Delta}_n)\cdot(\mathbf{R}^{(2)}+\mathbf{t}^{(2)})} \\ &= \frac{N\chi_{\alpha\beta}^2}{4\Omega}\sum_{\mathbf{G}^{(1)}\mathbf{G}^{(2)}\mathbf{G}\mathbf{q}nn'} J_{\mathbf{G}+\mathbf{q}}\delta_{\mathbf{G}+\mathbf{q},\mathbf{G}^{(1)}}\delta_{\mathbf{G}+\mathbf{q}+\boldsymbol{\Delta}_{n'}-\boldsymbol{\Delta}_n,\mathbf{G}^{(2)}}e^{i\mathbf{G}^{(1)}\cdot(\mathbf{t}^{(1)}-\mathbf{t}^{(2)})}e^{-i(\boldsymbol{\Delta}_{n'}-\boldsymbol{\Delta}_n)\cdot\mathbf{t}^{(2)}}. \end{aligned} \tag{B19}$$

We further sum over $\mathbf{G}\mathbf{q}$ obtaining

$$\frac{N\chi_{\alpha\beta}^2}{4\Omega}\sum_{\mathbf{G}^{(1)}\mathbf{G}^{(2)}nn'} J_{\mathbf{G}^{(1)}}\delta_{\mathbf{G}^{(1)},\mathbf{G}^{(2)}+\boldsymbol{\Delta}_n-\boldsymbol{\Delta}_{n'}}e^{i\mathbf{G}^{(1)}\cdot(\mathbf{t}^{(1)}-\mathbf{t}^{(2)})}e^{i(\boldsymbol{\Delta}_n-\boldsymbol{\Delta}_{n'})\cdot\mathbf{t}^{(2)}}. \tag{B20}$$

Since $\mathbf{G}^{(1)}$ and $\mathbf{G}^{(2)}$ differ only by a unit reciprocal lattice vector, the momentum conservation allows for the possibilities listed in Table II.

Using the delta function, we then obtain, depending on the sublattice indices, the following:

TABLE II. Combinations of summation variables that yield nonzero results in the sum (B20).

$\mathbf{G}^{(1)}$	$\mathbf{G}^{(2)}$	$\mathbf{G}^{(1)}-\mathbf{G}^{(2)}$	(n,n')
0	0	0	(1,1),(2,2),(3,3)
$\mathbf{G}_1^{(1)}$	$\mathbf{G}_1^{(2)}$	$\mathbf{G}_1^{\mathrm{M}}$	(2,1)
$\mathbf{G}_2^{(1)}$	$\mathbf{G}_2^{(2)}$	$\mathbf{G}_2^{\mathrm{M}}$	(3,1)
$\mathbf{G}_1^{(1)}-\mathbf{G}_2^{(1)}$	$\mathbf{G}_1^{(2)}-\mathbf{G}_2^{(2)}$	$\mathbf{G}_1^{\mathrm{M}}-\mathbf{G}_2^{\mathrm{M}}$	(2,3)
$-\mathbf{G}_1^{(1)}$	$-\mathbf{G}_1^{(2)}$	$-\mathbf{G}_1^{\mathrm{M}}$	(1,2)
$-\mathbf{G}_2^{(1)}$	$-\mathbf{G}_2^{(2)}$	$-\mathbf{G}_2^{\mathrm{M}}$	(1,3)
$-\mathbf{G}_1^{(1)}+\mathbf{G}_2^{(1)}$	$-\mathbf{G}_1^{(2)}+\mathbf{G}_2^{(2)}$	$-\mathbf{G}_1^{\mathrm{M}}+\mathbf{G}_2^{\mathrm{M}}$	(3,2)

(i) χ_{AA} terms ($\mathbf{t}^{(1)}=0,\mathbf{t}^{(2)}=0$) or χ_{BB} terms ($\mathbf{t}^{(1)}\neq 0,\mathbf{t}^{(2)}\neq 0$):

$$\frac{3N\chi_{\alpha\alpha}^2 J_{\mathrm{AA}}^{\mathbf{0}}}{4}+\frac{6N\chi_{\alpha\alpha}^2 J_{\mathrm{AA}}^{\mathbf{G}}}{4}, \tag{B21}$$

where $J_{\mathbf{k}=\mathbf{G}_1}=J_{\mathbf{k}=\mathbf{G}_2}=\ldots\equiv\Omega J^{\mathbf{G}}$;

(ii) χ_{AB} terms ($\mathbf{t}^{(1)}=0,\mathbf{t}^{(2)}\neq 0$) or χ_{BA} terms ($\mathbf{t}^{(1)}\neq 0,\mathbf{t}^{(2)}=0$):

$$\begin{aligned}&\frac{3N\chi_{AB}^2 J_{\mathrm{AB}}^{\mathbf{0}}}{4}+\frac{N\chi_{AB}^2 J_{\mathrm{AB}}^{\mathbf{G}}}{4}\left(e^{\mp i\mathbf{G}_1\cdot\mathbf{t}}+e^{\mp i\mathbf{G}_2\cdot\mathbf{t}}+e^{\mp i(\mathbf{G}_1+\mathbf{G}_2)\cdot\mathbf{t}}+\mathrm{c.c.}\right)\\&=\frac{3N\chi_{AB}^2 J_{\mathrm{AB}}^{\mathbf{0}}}{4}+\frac{N\chi_{AB}^2 J_{\mathrm{AB}}^{\mathbf{G}}}{4}\left(e^{\mp 2\pi i/3}+e^{\pm 2\pi i/3}+1+\mathrm{c.c.}\right)=\frac{3N\chi_{AB}^2 J_{\mathrm{AB}}^{\mathbf{0}}}{4}.\end{aligned} \tag{B22}$$

As the last ($\mathcal{N}$) term in (B2) can be treated analogously, this concludes the derivation of the continuum model of the twisted hexagonal Mott insulator. The complete versions of the model with $\mathbf{q}_n^J=0$ and $\mathbf{q}_n^J=\mathbf{\Delta}_n$ together with the mean-field equations are summarized below.

1. Uniform χ case

We write the mean-field Hamiltonian for the twisted hexagonal bilayer as a sum of the intralayer and the interlayer parts

$$\hat{H}_{\mathrm{u}}=\hat{H}^{\mathrm{intra}}+C^{\mathrm{intra}}+\hat{H}_{\mathrm{u}}^{\mathrm{inter}}+C_{\mathrm{u}}^{\mathrm{inter}}. \tag{B23}$$

We further perform on $\hat{H}_{\mathrm{u}}$ the gauge transformation with a unitary matrix

$$\mathcal{U}_{\delta\mathbf{p}\delta\mathbf{p}'}=\begin{pmatrix}\delta_{\delta\mathbf{p},\delta\mathbf{p}'-\mathbf{\Delta}_1/2}&0&0&0\\0&\delta_{\delta\mathbf{p},\delta\mathbf{p}'-\mathbf{\Delta}_1/2}&0&0\\0&0&\delta_{\delta\mathbf{p},\delta\mathbf{p}'+\mathbf{\Delta}_1/2}&0\\0&0&0&\delta_{\delta\mathbf{p},\delta\mathbf{p}'+\mathbf{\Delta}_1/2}\end{pmatrix} \tag{B24}$$

simultaneously with a shift of variables $\delta\mathbf{p}\to\delta\mathbf{p}-\mathbf{\Delta}_1/2$, $\delta\mathbf{p}'\to\delta\mathbf{p}'+\mathbf{\Delta}_1/2$. Just like in the Bistritzer-MacDonald model, in this basis, only the states in different layers with momenta that differ by $\mathbf{\Delta}_n$ can hybridize. This makes it convenient to parametrize

$$\delta\mathbf{p}=\mathbf{Q}+\mathbf{k},\quad \delta\mathbf{p}'=\mathbf{Q}'+\mathbf{k}, \tag{B25}$$

where $\mathbf{Q}$ and $\mathbf{Q}'$ belong to the different sublattices of the honeycomb lattice built on vectors $\mathbf{\Delta}_n$.

After this procedure, the intralayer term takes the form

$$(\hat{H}^{\mathrm{intra}})_{\mathbf{Q}\mathbf{Q}'}=\delta_{\mathbf{Q}\mathbf{Q}'}\sum_{\mathbf{k}}\hat{f}_{\mathbf{k}}^{\dagger}H^{\mathrm{intra}}(\mathbf{k})\hat{f}_{\mathbf{k}}, \tag{B26}$$

where

$$H^{\mathrm{intra}}(\mathbf{k})=\begin{pmatrix}\lambda-\mu_0&-\left(\delta t+\frac{\chi J}{4}\right)K_{\mathbf{k}}^{(1)}&0&0\\-\left(\delta t+\frac{\chi J}{4}\right)K_{\mathbf{k}}^{(1)}&\lambda-\mu_0&0&0\\0&0&\lambda-\mu_0&-\left(\delta t+\frac{\chi J}{4}\right)K_{\mathbf{k}}^{(2)}\\0&0&-\left(\delta t+\frac{\chi J}{4}\right)K_{\mathbf{k}}^{(2)}&\lambda-\mu_0\end{pmatrix}, \tag{B27}$$

and the rotated hopping matrices are

$$K_{\mathbf{k}}^{(l)}=v_F[R(\pm\theta/2)(\mathbf{k}+\mathbf{Q})\cdot(\hat{\sigma}_x,\hat{\sigma}_y)],\quad v_F=\tfrac{3}{2}at. \tag{B28}$$

The intralayer constant term is

$$C^{\text{intra}} = \frac{3}{2}NJ\chi^2 + \frac{N}{2}(1-\delta)(3\delta J - 8\lambda). \tag{B29}$$

The interlayer Hamiltonian can be cast as

$$(\hat{H}_{\text{u}}^{\text{inter}})_{\mathbf{Q}\mathbf{Q}'} = \sum_{\mathbf{k}\lambda} \hat{f}_{\mathbf{k}}^{\dagger}\left(H_1^{\text{inter}}\delta_{\mathbf{Q}'-\mathbf{Q},-\lambda\boldsymbol{\Delta}_1} + H_2^{\text{inter}}\delta_{\mathbf{Q}'-\mathbf{Q},-\lambda\boldsymbol{\Delta}_2} + H_3^{\text{inter}}\delta_{\mathbf{Q}'-\mathbf{Q},-\lambda\boldsymbol{\Delta}_3}\right)\hat{f}_{\mathbf{k}}, \tag{B30}$$

where the λ summation is over two values: $\lambda = +1$ corresponds to the hopping from layer 2 to layer 1, and $\lambda = -1$ in the opposite direction. We further define

$$H_i^{\text{inter}} = -\begin{pmatrix} 0 & 0 & \delta t_{\text{AA}} + \frac{\chi_{\text{AA}}J_{\text{AA}}}{4} & \omega^{i-1}\left(\delta t_{\text{AB}} + \frac{\chi_{\text{AB}}J_{\text{AB}}}{4}\right) \\ 0 & 0 & \omega^{-(i-1)}\left(\delta t_{\text{AB}} + \frac{\chi_{\text{AB}}J_{\text{AB}}}{4}\right) & \delta t_{\text{AA}} + \frac{\chi_{\text{BB}}J_{\text{AA}}}{4} \\ 0 & 0 & 0 & 0 \\ 0 & 0 & 0 & 0 \end{pmatrix}\delta_{\lambda,1} + (\text{H.c.})\delta_{\lambda,-1}. \tag{B31}$$

Lastly, the constant term arising from the interlayer tunneling and superexchange reads

$$C_{\text{u}}^{\text{inter}} = \frac{N}{4}\left(\chi_{\text{AA}}^2 + \chi_{\text{BB}}^2\right)J_{\text{AA}}^{\mathbf{0}} + \frac{N}{2}\chi_{\text{AB}}^2 J_{\text{AB}}^{\mathbf{0}} + \frac{N}{2}\delta(1-\delta)\left(J_{\text{AA}}^{\mathbf{0}} + J_{\text{AB}}^{\mathbf{0}}\right). \tag{B32}$$

The mean-field equations for χ, χ_{AA}, χ_{BB}, χ_{AB}, λ, and δ obtained by minimizing (B23) are as follows:

$$\chi = \frac{1}{6}\sum_{\mathbf{Q},\,E_n<E_F}\int\frac{d^2\mathbf{k}}{K}\,\langle n\mathbf{k}\mathbf{Q}|\hat{H}^{\text{intra}}|n\mathbf{k}\mathbf{Q}\rangle\,, \quad \chi_{\text{AA(BB)}} = \frac{J_{\text{AA}}}{J_{\text{AA}}^{\mathbf{0}}}\sum_{\mathbf{Q},\,E_n<E_F}\int\frac{d^2\mathbf{k}}{K}\,\langle n\mathbf{k}\mathbf{Q}|\hat{H}_{\text{u}}^{\text{AA(BB)}}|n\mathbf{k}\mathbf{Q}\rangle\,,$$

$$\chi_{\text{AB}} = \frac{J_{\text{AB}}}{2J_{\text{AB}}^{\mathbf{0}}}\sum_{\mathbf{Q},\,E_n<E_F}\int\frac{d^2\mathbf{k}}{K}\,\langle n\mathbf{k}\mathbf{Q}|\hat{H}_{\text{u}}^{\text{AB}}|n\mathbf{k}\mathbf{Q}\rangle\,, \quad \delta = 1 - \frac{1}{2}\sum_{\mathbf{Q},E_n<E_F}\int\frac{d^2\mathbf{k}}{K}\,\langle n\mathbf{k}\mathbf{Q}|\hat{H}_{\text{u}}|n\mathbf{k}\mathbf{Q}\rangle\,,$$

$$\lambda = 3t\chi + \frac{t_{\text{AA}}}{2}\frac{J_{\text{AA}}^{\mathbf{0}}}{J_{\text{AA}}}(\chi_{\text{AA}} + \chi_{\text{BB}}) + \frac{2J_{\text{AB}}^{\mathbf{0}}}{J_{\text{AB}}}\frac{t_{\text{AB}}}{2}\chi_{\text{AB}} - \frac{1}{8}(1-2\delta)\left(3J + J_{\text{AA}}^{\mathbf{0}} + J_{\text{AB}}^{\mathbf{0}}\right), \tag{B33}$$

where

$$(\hat{H}^{\text{intra}})_{\mathbf{Q}\mathbf{Q}'} = \delta_{\mathbf{Q}\mathbf{Q}'}\sum_{\mathbf{k}}\hat{f}_{\mathbf{k}}^{\dagger}\begin{pmatrix} 0 & K_{\mathbf{k}}^{(1)} & 0 & 0 \\ K_{\mathbf{k}}^{(1)} & 0 & 0 & 0 \\ 0 & 0 & 0 & K_{\mathbf{k}}^{(2)} \\ 0 & 0 & K_{\mathbf{k}}^{(2)} & 0 \end{pmatrix}f_{\mathbf{k}}^{\dagger}, \tag{B34}$$

and

$$\left(\hat{H}_{\text{u}}^{\text{AA(BB,AB)}}\right)_{\mathbf{Q}\mathbf{Q}'} = \sum_{\mathbf{k}\lambda}\hat{f}_{\mathbf{k}}^{\dagger}\left(H_1^{\text{AA(BB,AB)}}\delta_{\mathbf{Q}'-\mathbf{Q},-\lambda\boldsymbol{\Delta}_1} + H_2^{\text{AA(BB,AB)}}\delta_{\mathbf{Q}'-\mathbf{Q},-\lambda\boldsymbol{\Delta}_2} + H_3^{\text{AA(BB,AB)}}\delta_{\mathbf{Q}'-\mathbf{Q},-\lambda\boldsymbol{\Delta}_3}\right)\hat{f}_{\mathbf{k}}, \tag{B35}$$

where, finally,

$$H_i^{\text{AA}} = \begin{pmatrix} 0 & 0 & 1 & 0 \\ 0 & 0 & 0 & 0 \\ 0 & 0 & 0 & 0 \\ 0 & 0 & 0 & 0 \end{pmatrix}\delta_{\lambda,1} + (\text{H.c.})\delta_{\lambda,-1}, \quad H_i^{\text{BB}} = \begin{pmatrix} 0 & 0 & 0 & 0 \\ 0 & 0 & 0 & 1 \\ 0 & 0 & 0 & 0 \\ 0 & 0 & 0 & 0 \end{pmatrix}\delta_{\lambda,1} + (\text{H.c.})\delta_{\lambda,-1},$$

$$H_i^{\text{AB}} = \begin{pmatrix} 0 & 0 & 0 & \omega^{i-1} \\ 0 & 0 & \omega^{-(i-1)} & 0 \\ 0 & 0 & 0 & 0 \\ 0 & 0 & 0 & 0 \end{pmatrix}\delta_{\lambda,1} + (\text{H.c.})\delta_{\lambda,-1}. \tag{B36}$$

2. Spatially dependent χ case

We keep the same gauge as in the uniform case and present the Hamiltonian as below:

$$\hat{H}_{\text{nu}} = \hat{H}^{\text{intra}} + C^{\text{intra}} + \hat{H}_{\text{nu}}^{\text{inter}} + C_{\text{nu}}^{\text{inter}}. \tag{B37}$$

The third term in this expression is

$$\left(H_{\rm nu}^{\rm inter}\right)_{\mathbf{QQ}'} = \sum_{\mathbf{k}\lambda n} \hat{f}^\dagger_{\mathbf{k}} \left(H^{\rm inter}_{1,J}\delta_{\mathbf{Q}'-\mathbf{Q},-\lambda(\mathbf{\Delta}_1-\mathbf{\Delta}_n)} + H^{\rm inter}_{2,J}\delta_{\mathbf{Q}'-\mathbf{Q},-\lambda(\mathbf{\Delta}_2-\mathbf{\Delta}_n)} + H^{\rm inter}_{3,J}\delta_{\mathbf{Q}'-\mathbf{Q},-\lambda(\mathbf{\Delta}_3-\mathbf{\Delta}_n)}\right)\hat{f}_{\mathbf{k}} + \hat{H}^{\rm inter}_{{\rm nu},t}, \tag{B38}$$

where we defined

$$H^{\rm inter}_{i,J} = H^{\rm inter}_i\big|_{\delta\to 0}, \quad \hat{H}^{\rm inter}_{{\rm nu},t} = \hat{H}^{\rm inter}_{\rm u}\big|_{J_{\rm AA},J_{\rm AB}\to 0}. \tag{B39}$$

The crucial novelty introduced by the presence of extra $\mathbf{\Delta}_n$ in (B38) is the possibility of hybridization between two Dirac cones from different layers at the momenta $\mathbf{\Delta}_n - \mathbf{\Delta}_m$. This necessitates promoting $\mathbf{Q}$ and $\mathbf{Q}'$ to the coordinates of the vertices belonging to the *triangular* lattice spanned by vectors $\mathbf{\Delta}_n$, which are the reciprocal lattice vectors in this model. This change makes the area of the Brillouin zone three times smaller than in the uniform order parameter case solved on a honeycomb lattice spanned by the same vectors. Consequently, the size of the moiré unit cell in the real space becomes three times larger. Lastly, the constant coming from the interlayer hopping is $C^{\rm inter}_{\rm nu} = \frac{3N}{4}(J^{\mathbf{0}}_{\rm AA} + 2J^{\mathbf{G}}_{\rm AA})(\chi^2_{\rm AA} + \chi^2_{\rm BB}) + \frac{3N}{2}\chi^2_{\rm AB}J^{\mathbf{0}}_{\rm AB} + \frac{N}{2}\delta(1-\delta)(J^{\mathbf{0}}_{\rm AA} + J^{\mathbf{0}}_{\rm AB})$. The mean-field equations for χ, $\chi_{\rm AA}$, $\chi_{\rm BB}$, $\chi_{\rm AB}$, λ, and δ are only slightly modified compared to the case with the uniform order parameter (B34),

$$\chi = \frac{1}{6}\sum_{\mathbf{Q},\,E_n<E_F}\int \frac{d^2\mathbf{k}}{K}\,\langle n\mathbf{kQ}|\hat{H}^{\rm intra}|n\mathbf{kQ}\rangle\,, \quad \chi_{\rm AA(BB)} = \frac{J_{\rm AA}}{3\left(J^{\mathbf{0}}_{\rm AA} + 2J^{\mathbf{G}}_{\rm AA}\right)}\sum_{\mathbf{Q},\,E_n<E_F}\int \frac{d^2\mathbf{k}}{K}\,\langle n\mathbf{kQ}|\hat{H}^{\rm AA(BB)}_{\rm nu}|n\mathbf{kQ}\rangle\,,$$

$$\chi_{\rm AB} = \frac{J_{\rm AB}}{6J^{\mathbf{0}}_{\rm AB}}\sum_{\mathbf{Q},\,E_n<E_F}\int \frac{d^2\mathbf{k}}{K}\,\langle n\mathbf{kQ}|\hat{H}^{\rm AB}_{\rm nu}|n\mathbf{kQ}\rangle\,, \quad \delta = 1 - \frac{1}{2}\sum_{\mathbf{Q},E_n<E_F}\int \frac{d^2\mathbf{k}}{K}\,\langle n\mathbf{kG}_M|\hat{H}_{\rm nu}|n\mathbf{kQ}\rangle\,,$$

$$\lambda = 3t\chi + \frac{t_{\rm AA}}{2}\frac{3(J^{\mathbf{0}}_{\rm AA} + 2J^{\mathbf{G}}_{\rm AA})}{J_{\rm AA}}(\chi_{\rm AA} + \chi_{\rm BB}) + \frac{t_{\rm AB}}{2}\frac{6J^{\mathbf{0}}_{\rm AB}}{J_{\rm AB}}\chi_{\rm AB} - \frac{1}{8}(1-2\delta)\left(3J + J^{\mathbf{0}}_{\rm AA} + J^{\mathbf{0}}_{\rm AB}\right), \tag{B40}$$

with

$$\left(\hat{H}^{\rm AA(BB,AB)}_{\rm nu}\right)_{\mathbf{QQ}'} = \sum_{\mathbf{k}\lambda}\hat{f}^\dagger_{\mathbf{k}}\left(H^{\rm AA(BB,AB)}_1\delta_{\mathbf{Q}'-\mathbf{Q},\,-\lambda(\mathbf{\Delta}_1-\mathbf{\Delta}_n)} + H^{\rm AA(BB,AB)}_2\delta_{\mathbf{Q}'-\mathbf{Q},\,-\lambda(\mathbf{\Delta}_2-\mathbf{\Delta}_n)} + H^{\rm AA(BB,AB)}_3\delta_{\mathbf{Q}'-\mathbf{Q},\,-\lambda(\mathbf{\Delta}_3-\mathbf{\Delta}_n)}\right)\hat{f}_{\mathbf{k}}. \tag{B41}$$

APPENDIX C: SYMMETRIES OF THE NONUNIFORM χ MODEL

The symmetries of the BM model are well known [40]. In our model, on the other hand, we leave the possibility for the mismatch in the momentum dependence between the terms responsible for the interlayer tunneling (denoted with t) and the interlayer superexchange (denoted with J). Both types of terms can be cast in the form

$$(H_{\rm inter})^{t(J)}_{\delta\mathbf{p}\delta\mathbf{p}'} = \sum_{\mathbf{k}\lambda nm}\hat{f}^\dagger_{\delta\mathbf{p}}H^{t(J)}_{{\rm inter},m\lambda}\hat{f}_{\delta\mathbf{p}'}\delta_{\delta\mathbf{p}'-\delta\mathbf{p},\,-\lambda(\mathbf{\Delta}_m-\mathbf{q}^{t(J)}_n)}, \quad H^t_{{\rm inter},m\lambda} = -\begin{pmatrix}0 & T^t_m\\ 0 & 0\end{pmatrix}\delta_{\lambda,1} + ({\rm H.c.})\delta_{\lambda,-1},$$

$$H^J_{{\rm inter},m\lambda} = -\begin{pmatrix}0 & T^J_m\\ 0 & 0\end{pmatrix}\delta_{\lambda,1} + ({\rm H.c.})\delta_{\lambda,-1}, \quad T^t_m = \begin{pmatrix}\delta t_{\rm AA} & \omega^{m-1}\delta t_{\rm AB}\\ \omega^{-(m-1)}\delta t_{\rm AB} & \delta t_{\rm AA}\end{pmatrix}, \quad T^J_m = \begin{pmatrix}\frac{\chi_{\rm AA}J_{\rm AA}}{4} & \omega^{m-1}\frac{\chi_{\rm AB}J_{\rm AB}}{4}\\ \omega^{-(m-1)}\frac{\chi_{\rm AB}J_{\rm AB}}{4} & +\frac{\chi_{\rm BB}J_{\rm AA}}{4}\end{pmatrix}. \tag{C1}$$

Furthermore, both interlayer terms can be diagonalized by performing the Fourier transform over $\delta\mathbf{p}$ and $\delta\mathbf{p}'$, which yields

$$(H_{\rm inter})^{t(J)} = \sum_{j\lambda nm}\hat{f}^\dagger_j H^{t(J)}_{{\rm inter},m\lambda}\hat{f}_j e^{i(\mathbf{\Delta}_m - \mathbf{q}^{t(J)}_n)\cdot\mathbf{j}}. \tag{C2}$$

Let us consider how the moiré translation symmetry acts on the sum $(H_{\rm inter})^t + (H_{\rm inter})^J$. The interlayer hopping term in our model has a trivial momentum dependence, i.e., $\mathbf{q}^t_n = 0$. Therefore, if the interlayer superexchange term has no momentum dependence as well ($\mathbf{q}^J_n = 0$), the translational symmetry of the Hamiltonian that includes the sum of $(H_{\rm inter})^t$ and $(H_{\rm inter})^J$ is identical to that in the Bistritzer-MacDonald model. Hence, moiré translations are a good symmetry in this case.

Now suppose $\mathbf{q}^J_n = \mathbf{\Delta}_n$. Consider performing a coordinate transformation by shifting $\mathbf{j}$ by one of the moiré lattice vectors $\mathbf{a}_1 = 3a/(2\theta)(1,\,1/\sqrt{3})$. Since $e^{\mathbf{a}_1\cdot\mathbf{\Delta}_n} = \omega$, and $e^{\mathbf{a}_1\cdot(\mathbf{\Delta}_n - \mathbf{\Delta}_m)} = 1$, the term $(H_{\rm inter})^t$ acquires the additional phase equal to ω under moiré translation, whereas the interlayer superexchange $(H_{\rm inter})^J$ stays invariant. If the superexchange term was absent, one could have performed a gauge transformation with the matrix

$$\mathcal{M} = \begin{pmatrix}\omega^{1/2} & 0 & 0 & 0\\ 0 & \omega^{1/2} & 0 & 0\\ 0 & 0 & \omega^{-1/2} & 0\\ 0 & 0 & 0 & \omega^{-1/2}\end{pmatrix}, \tag{C3}$$

which would have restored $(H_{\rm inter})^t$ to the original form. If, on the other hand, both superexchange and the hopping terms are

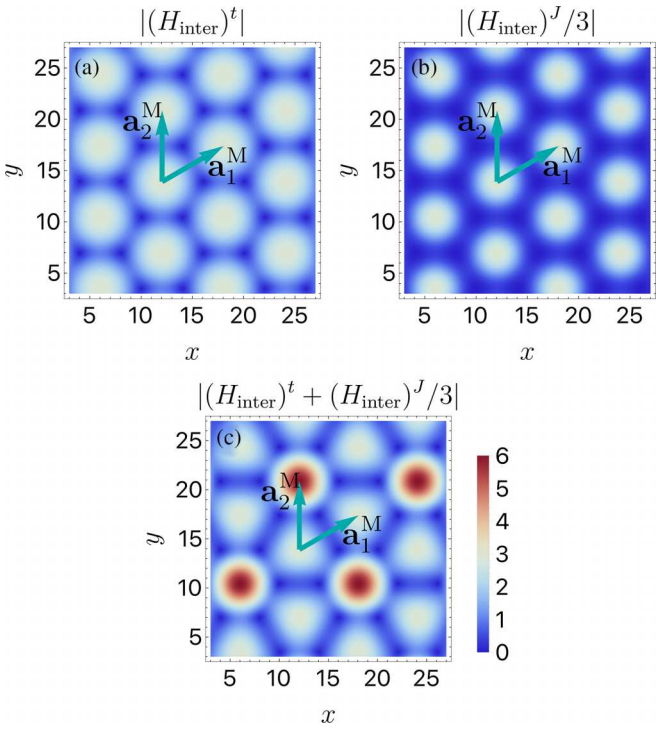

FIG. 7. Textures in the real space corresponding to the terms $|(H_{\text{inter}})^t|$ (a), $|(H_{\text{inter}})^J/3|$ (b), and their interference pattern $|(H_{\text{inter}})^t + (H_{\text{inter}})^J/3|$ (c). The moiré lattice vectors $\mathbf{a}^{\text{M}}_{1,2}$ are indicated with blue arrows. As one can infer from the figures, the first two terms are moiré-periodic, whereas the latter breaks moiré translations.

present, this gauge transformation cannot bring their sum to the original form. Therefore, having $\mathbf{q}_n^J = \mathbf{\Delta}_n$ simultaneously with $\delta \neq 0$ lowers the translation symmetry. The new translation vectors $\mathbf{d}_1 = 2a/(2\theta)(1, 1/\sqrt{3})$, $\mathbf{d}_2 = (3a/\theta, 0)$ are the reciprocal lattice vectors with respect to $\mathbf{\Delta}_n$, since in this case $e^{\mathbf{d}_i \cdot \mathbf{\Delta}_n} = e^{\mathbf{d}_i \cdot \mathbf{G}_n^{\text{M}}} = 1$, and such translation does not produce any phases. This argument can be visualized by considering the textures in the real space produced by the terms $|(H_{\text{inter}})^t|$, $|(H_{\text{inter}})^J/3|$, and $|(H_{\text{inter}})^t + (H_{\text{inter}})^J/3|$ with all the constant prefactors in these terms such as δt_{AA} or $\chi_{\text{AA}} J_{\text{AA}}/4$ set to unity. As one can see from Fig. 7, the former two terms produce a moiré-periodic pattern in real space, whereas the latter breaks moiré translations.

Besides the moiré translations, in our model, the C_2 symmetry can also be broken if $\chi_{\text{AA}} \neq \chi_{\text{BB}}$. In order for $(H_{\text{inter}})^J$ to be invariant under C_2, one requires [40]

$$\sigma_x T_1^J \sigma_x = T_1^J, \quad \sigma_x T_2^J \sigma_x = T_3^J. \tag{C4}$$

Since the hopping matrix interchanges both the diagonal and off-diagonal entries and the off-diagonal terms are self-consistently found to be equal across all phases, the case $\chi_{\text{AA}} = \chi_{\text{BB}}$ preserves this symmetry and $\chi_{\text{AA}} \neq \chi_{\text{BB}}$ breaks.

APPENDIX D: COMPARISON WITH THE UNTWISTED CASE AND TWIST ANGLE DEPENDENCE

In this Appendix, we compare the model of the untwisted correlated bilayer introduced in Appendix A and the model describing the correlated twisted bilayer obtained in Appendix B.

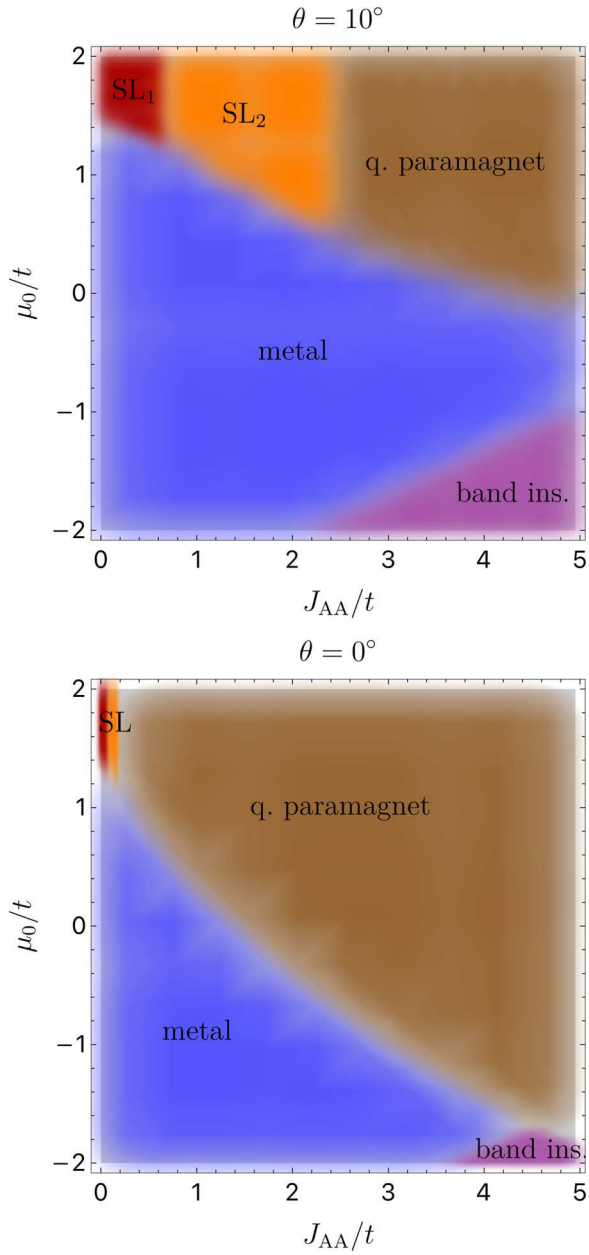

FIG. 8. The comparison of the phase diagram between the $\theta = 10°$ (top) and the untwisted case (on the bottom). The band insulator phase is characterized by $\delta = 1$; i.e., no spinons are present in the system. The parameters used to obtain the diagrams are matched according to the procedure outlined in Appendix D. The variables not fixed by matching are the same as in Fig. 3. We note that for the values of parameters used, no excitonic insulator phase is found due to the large ratio $J^0_{\text{AA}}/J_{\text{AA}}$ required for matching.

Let us consider as a starting point the untwisted case defined in the full hexagonal Brillouin zone (BZ). The matching onto the continuous model is performed by dividing the Brillouin zone into two Dirac cones with the conservation of the number of states

$$\int_{\text{BZ}} \frac{d^2\mathbf{k}\, A}{(2\pi)^2} = 2 \int_{|\mathbf{k}|<R} \frac{d^2\mathbf{k}\, A}{(2\pi)^2}. \tag{D1}$$

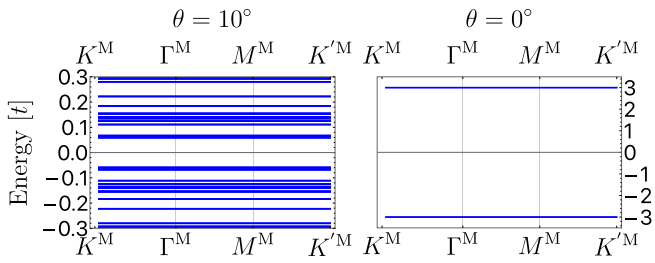

FIG. 9. Band structure in the quantum paramagnet case with $\theta = 10^\circ$ (on the left) and $\theta = 0^\circ$ (on the right). The parameters used correspond to the $J_{AA} = 4t$, $\mu = 1.5t$ in the phase diagrams in Fig. 8.

Therefore,

$$\frac{8\pi^2 a^2}{3\sqrt{3}} = 2\pi R^2 \rightarrow R = \sqrt{\frac{4\pi}{3\sqrt{3}}}a. \tag{D2}$$

We expect this truncation of the Brillouin zone to introduce some errors, which we discuss further below.

The next step is to match the full untwisted Hamiltonian [Eq. (A9)] with both the uniform [Eq. (B23)] and nonuniform [Eq. (B37)] cases. The uniform model reduces to the untwisted case if, with $\theta = 0$, we simultaneously set $J^{\mathbf{0}}_{AA} = 3J_{AA}$. We also need to use $\chi_{AB} = 0$ and $J^{\mathbf{0}}_{AB} = 0$, $t_{AB} = 0$ which ensures that no traces of AB superexchange remain. It can be further seen in the nonuniform case that up to the redefinition of χ_{AA} and χ_{BB}, the Hamiltonian for the untwisted bilayer can be reproduced by setting $J^{\mathbf{0}}_{AA} = J^{\mathbf{G}}_{AA} = 3J_{AA}$, $\chi_{AB} = 0$, $J^{\mathbf{0}}_{AB} = 0$.

We immediately note that the nature of the interlayer hybridization is completely different in the $\theta = 0$ and $\theta \simeq 0$ cases, and no smooth crossover exists between the two. In the former case, the gap may open only at neutrality, whereas in the latter, the minibands hybridize with each other, and many gaps are present at the same time. Therefore, whenever interlayer hybridization is important, we expect considerable differences between the twisted and untwisted cases, even at small angles, whereas the properties of the less reliant on the existence of the gaps metallic phase should be relatively similar.

This intuition is confirmed by the numerical simulations, as seen in Fig. 8. We observe that the quantum paramagnet phase in the twisted case occupies a much smaller fraction of the diagram due to the difference in the hybridization pattern: two remote flat bands occur in the $\theta = 0^\circ$ case, whereas multiple

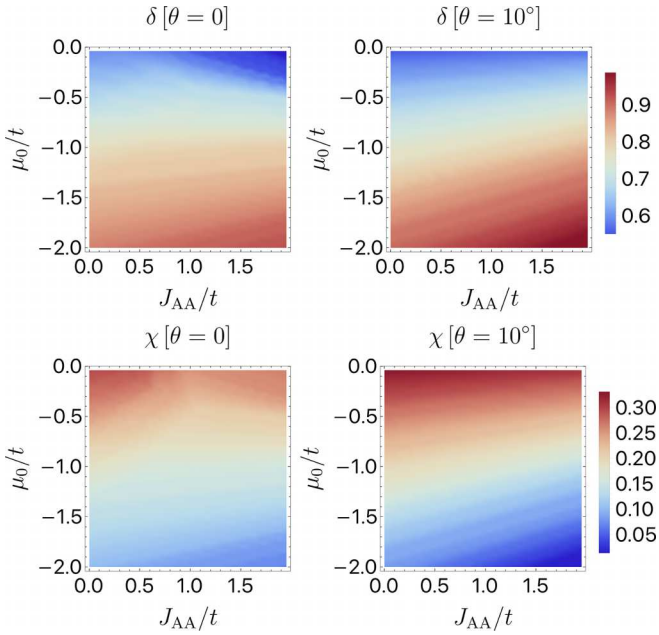

FIG. 10. Comparison of mean-field parameters δ and χ between the metallic phases in the twisted and untwisted cases in Fig. 8. The quantities agree well between $\theta = 10^\circ$ and $\theta = 0^\circ$ cases, which justifies the matching procedure.

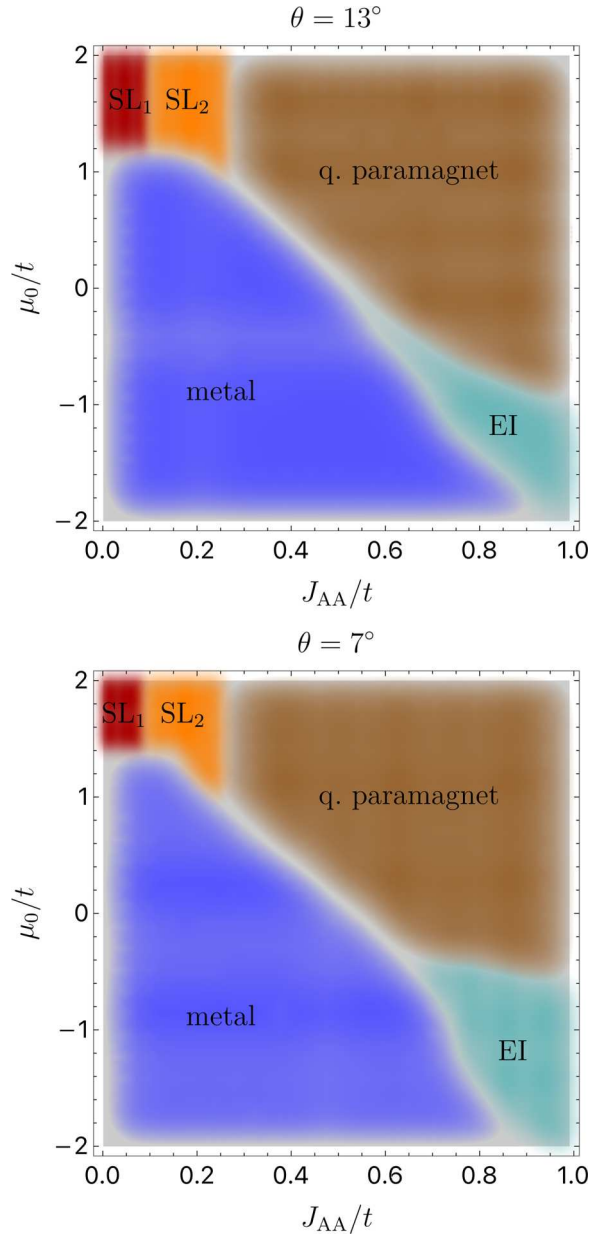

FIG. 11. Phase diagrams obtained for the same set of parameters as used in Fig. 3 but for different twist angles: $\theta = 13^\circ$ on the top and $\theta = 7^\circ$ on the bottom.

flat bands exist in $\theta = 10^\circ$ case, as shown in Fig. 9. The latter configuration is much less efficient in minimizing the interlayer part of the energy as the gap is effectively smaller. We also point out that for the same reason, the spin liquid phases are almost absent on the $\theta = 0^\circ$ diagram, whereas the twisted case features such phases.

As we expected, the metallic phases in both cases show very similar properties as follows from the Fig. 10 in which the parameters δ and χ are compared between the twisted ($\theta = 10^\circ$) and the untwisted cases. From this, we conclude that the truncation of the Brillouin zone down to two circles surrounding the Dirac points does not qualitatively affect our results.

Lastly, we comment on the twist angle variation of the phase diagram: the phase diagrams for $\theta = 13^\circ$ and $\theta = 7^\circ$ are shown in Fig. 11. One would expect that the lower the twist angle is, the more minibands there are, and the opportunity to stabilize the gapped EI phase characterized by the small but nonzero δ is increasing. This trend is seen among the calculated phase diagrams presented in Fig. 11: the EI phase is the only one essentially sensitive to the increase of the twist angle and would eventually disappear as θ is increased. The reason is that at the large twist angle, only two Dirac cones within the cutoff radius R remain, and the minibands are absent. Therefore, the phase diagram at large θ essentially becomes the one corresponding to the untwisted case.

[1] Y. Cao, V. Fatemi, S. Fang, K. Watanabe, T. Taniguchi, E. Kaxiras, and P. Jarillo-Herrero, Unconventional superconductivity in magic-angle graphene superlattices, Nature (London) **556**, 43 (2018).

[2] A. Jorio, Twistronics and the small-angle magic, Nat. Mater. **21**, 844 (2022).

[3] L. Wang, E.-M. Shih, A. Ghiotto, L. Xian, D. A. Rhodes, C. Tan, M. Claassen, D. M. Kennes, Y. Bai, B. Kim, K. Watanabe, T. Taniguchi, X. Zhu, J. Hone, A. Rubio, A. N. Pasupathy, and C. R. Dean, Correlated electronic phases in twisted bilayer transition metal dichalcogenides, Nat. Mater. **19**, 861 (2020).

[4] A. M. Seiler, F. R. Geisenhof, F. Winterer, K. Watanabe, T. Taniguchi, T. Xu, F. Zhang, and R. T. Weitz, Quantum cascade of correlated phases in trigonally warped bilayer graphene, Nature (London) **608**, 298 (2022).

[5] S. Paschen and Q. Si, Quantum phases driven by strong correlations, Nat. Rev. Phys. **3**, 9 (2021).

[6] P. A. Lee, N. Nagaosa, and X.-G. Wen, Doping a Mott insulator: Physics of high temperature superconductivity, Rev. Mod. Phys. **78**, 17 (2006).

[7] P. Coleman, C. Pépin, Q. Si, and R. Ramazashvili, How do Fermi liquids get heavy and die?, J. Phys.: Condens. Matter **13**, R723 (2001).

[8] Z.-D. Song and B. A. Bernevig, Magic-angle twisted bilayer graphene as a topological heavy fermion problem, Phys. Rev. Lett. **129**, 047601 (2022).

[9] K. Hejazi, Z.-X. Luo, and L. Balents, Noncollinear phases in moiré magnets, Proc. Natl. Acad. Sci. USA **117**, 10721 (2020).

[10] M. Akram and O. Erten, Skyrmions in twisted van der Waals magnets, Phys. Rev. B **103**, L140406 (2021).

[11] K. Hejazi, Z.-X. Luo, and L. Balents, Heterobilayer moiré magnets: Moiré skyrmions and commensurate-incommensurate transitions, Phys. Rev. B **104**, L100406 (2021).

[12] M. Akram, H. LaBollita, D. Dey, J. Kapeghian, O. Erten, and A. S. Botana, Moiré skyrmions and chiral magnetic phases in twisted CrX_3 (X = I, Br, and Cl) bilayers, Nano Lett. **21**, 6633 (2021).

[13] E. M. Nica, M. Akram, A. Vijayvargia, R. Moessner, and O. Erten, Kitaev spin-orbital bilayers and their moiré superlattices, npj Quantum Mater. **8**, 9 (2023).

[14] K.-M. Kim, D. H. Kiem, G. Bednik, M. J. Han, and M. J. Park, *Ab initio* spin Hamiltonian and topological noncentrosymmetric magnetism in twisted bilayer CrI_3, Nano Lett. **23**, 6088 (2023).

[15] M. Akram, J. Kapeghian, J. Das, R. Valentí, A. S. Botana, and O. Erten, Theory of moiré magnetism in twisted bilayer α-$RuCl_3$, Nano Lett. **24**, 890 (2024).

[16] M. A. Keskiner, P. Ghaemi, M. Ö. Oktel, and O. Erten, Theory of moiré magnetism and multidomain spin textures in twisted Mott insulator–semimetal heterobilayers, Nano Lett. **24**, 8575 (2024).

[17] J. Das and O. Erten, Moiré-mediated phases in synthetic Kondo superlattices, arXiv:2408.05324.

[18] Y. Xu, A. Ray, Y.-T. Shao, S. Jiang, K. Lee, D. Weber, J. E. Goldberger, K. Watanabe, T. Taniguchi, D. A. Muller, K. F. Mak, and J. Shan, Coexisting ferromagnetic-antiferromagnetic state in twisted bilayer CrI_3, Nat. Nanotechnol. **17**, 143 (2022).

[19] T. Song, Q.-C. Sun, E. Anderson, C. Wang, J. Qian, T. Taniguchi, K. Watanabe, M. A. McGuire, R. Stöhr, D. Xiao, T. Cao, J. Wrachtrup, and X. Xu, Direct visualization of magnetic domains and moire magnetism in twisted 2D magnets, Science **374**, 1140 (2021).

[20] H. Xie, X. Luo, Z. Ye, Z. Sun, G. Ye, S. Sung, H. Ge, S. Yan, Y. Fu, S. Tian, H. Lei, K. Sun, R. Hovden, R. He, and L. Zhao, Evidence of non-collinear spin texture in magnetic moiré superlattices, Nat. Phys. **19**, 1150 (2023).

[21] T. Tummuru, S. Plugge, and M. Franz, Josephson effects in twisted cuprate bilayers, Phys. Rev. B **105**, 064501 (2022).

[22] P. M. Eugenio, Z.-X. Luo, A. Vishwanath, and P. A. Volkov, Tunable t-t'-U Hubbard models in twisted square homobilayers, arXiv:2406.02448.

[23] S. Y. F. Zhao, X. Cui, P. A. Volkov, H. Yoo, S. Lee, J. A. Gardener, A. J. Akey, R. Engelke, Y. Ronen, R. Zhong, G. Gu, S. Plugge, T. Tummuru, M. Kim, J. H. Pixley, and P. Kim, Time-reversal symmetry breaking superconductivity between twisted cuprate superconductors, Science **382**, 1422 (2023).

[24] Y.-B. Liu, J. Zhou, C. Wu, and F. Yang, Charge-4e superconductivity and chiral metal in 45°-twisted bilayer cuprates and related bilayers, Nat. Commun. **14**, 7926 (2023).

[25] X. Lu and D. Sénéchal, Doping phase diagram of a Hubbard model for twisted bilayer cuprates, Phys. Rev. B **105**, 245127 (2022).

[26] H.-K. Tang, J. N. Leaw, J. N. B. Rodrigues, I. F. Herbut, P. Sengupta, F. F. Assaad, and S. Adam, The role of

electron-electron interactions in two-dimensional Dirac fermions, Science **361**, 570 (2018).
[27] K. A. Chao, J. Spalek, and A. M. Oles, Canonical perturbation expansion of the Hubbard model, Phys. Rev. B **18**, 3453 (1978).
[28] Z.-T. Xu, Z.-C. Gu, and S. Yang, Competing orders in the honeycomb lattice *t-J* model, Phys. Rev. B **108**, 035144 (2023).
[29] M. Blei, J. L. Lado, Q. Song, D. Dey, O. Erten, V. Pardo, R. Comin, S. Tongay, and A. S. Botana, Synthesis, engineering, and theory of 2D van der Waals magnets, Appl. Phys. Rev. **8**, 021301 (2021).
[30] N. Bultinck, S. Chatterjee, and M. P. Zaletel, Mechanism for anomalous Hall ferromagnetism in twisted bilayer graphene, Phys. Rev. Lett. **124**, 166601 (2020).
[31] R. Bistritzer and A. H. MacDonald, Moiré bands in twisted double-layer graphene, Proc. Natl. Acad. Sci. USA **108**, 12233 (2011).
[32] P. Coleman, *Introduction to Many-Body Physics* (Cambridge University Press, 2015).
[33] D. K. Efimkin and A. H. MacDonald, Helical network model for twisted bilayer graphene, Phys. Rev. B **98**, 035404 (2018).
[34] D. Jérome, T. M. Rice, and W. Kohn, Excitonic insulator, Phys. Rev. **158**, 462 (1967).
[35] P. Coleman, New approach to the mixed-valence problem, Phys. Rev. B **29**, 3035 (1984).
[36] A. Vijayvargia and O. Erten, Nematic heavy fermions and coexisting magnetic order in CeSiI, Phys. Rev. B **109**, L201118 (2024).
[37] L. Lilly, A. Muramatsu, and W. Hanke, Slave-boson mean field versus quantum Monte Carlo results for the Hubbard model, Phys. Rev. Lett. **65**, 1379 (1990).
[38] T.-H. Lee, N. Lanatà, and G. Kotliar, Accuracy of ghost rotationally invariant slave-boson and dynamical mean field theory as a function of the impurity-model bath size, Phys. Rev. B **107**, L121104 (2023).
[39] D. Riegler, M. Klett, T. Neupert, R. Thomale, and P. Wölfle, Slave-boson analysis of the two-dimensional Hubbard model, Phys. Rev. B **101**, 235137 (2020).
[40] B. A. Bernevig, Derivation of the Bistritzer-MacDonald Hamiltonian, 2019, http://tms19.dipc.org/wp-content/uploads/2019/11/SummerSchoolDonostia2019_BERNEVIG.pdf.